DNA damage and somatic mutations engraved on the genomes of mammalian cells after irradiation with a nail polish dryer

Maria Zhivagui[1-3], Areebah Hoda[1], Noelia Valenzuela[3], Yi-Yu Yeh[2], Jason Dai[2], Yudou He[1-3], Bennett Van Houten[4], and Ludmil B. Alexandrov[1-3*]

Affiliations

[1]Department of Cellular and Molecular Medicine, UC San Diego, La Jolla, CA, 92093, USA

[2]Department of Bioengineering, UC San Diego, La Jolla, CA, 92093, USA

[3]Moores Cancer Center, UC San Diego, La Jolla, CA, 92037, USA

[4]UPMC-Hillman Cancer Center, University of Pittsburgh, PA 15213

[*]Correspondence should be addressed to L2alexandrov@health.ucsd.edu.

ABSTRACT

Ultraviolet A light (UVA) is commonly emitted by nail polish dryers with recent reports suggesting that long-term use of UV-nail polish dryers may increase the risk for developing skin cancer. However, no experimental evaluation has been conducted to reveal the effect of radiation emitted by UV-nail polish dryers on mammalian cells. Here, we examine the DNA damage and somatic mutations found on the genomes of human and murine cells due to irradiation by a UV-nail dryer. High levels of reactive oxygen species were observed in all UVA-irradiated samples, consistent with elevated 8-oxo-7,8-dihydroguanine damage and mitochondrial dysfunction. Analysis of somatic mutations revealed a dose-dependent increase of C:G>A:T substitutions in irradiated samples with a pattern similar to the ones of COSMIC signatures SBS18/36, mutational signatures attributed to reactive oxygen species. Re-examination of previously generated skin cancer genomics data revealed that SBS18/36 are ubiquitously present in melanoma and account for ~12% of the observed driver mutations. In summary, this study demonstrates that radiation emitted by UV-nail polish dryers can both damage DNA and permanently engrave somatic mutations on the genomes of mammalian cells. These results have far-reaching implications in regard to public health and to preventing skin cancer due to occupational- or consumer-based exposure to ultraviolet light from artificial sources.

38 **INTRODUCTION**

39 Ultraviolet (UV) light is a type of electromagnetic radiation with a wavelength ranging between
40 10nm and 400nm. Since wavelengths below 280nm are generally blocked by the Earth's
41 stratospheric ozone, the UV light that reaches the Earth's surface is between 280nm and 400nm[1].
42 The UV spectrum can be further categorized based on its effect on human skin as well as on its
43 ability to induce DNA damage[2]. Ultraviolet B light (UVB; 280-315nm) accounts for about 10%
44 of the UV found on Earth, penetrates the outer layer of the skin, and it induces a plethora of DNA
45 lesions including cyclobutane-pyrimidine dimers and 6-4 photoproducts[3,4]. In contrast, ultraviolet
46 A light (UVA; 315-400nm) constitutes approximately 90% of the ultraviolet radiation that reaches
47 the surface of the Earth, it can penetrate the skin more deeply, and it causes little direct DNA
48 damage as UVA is poorly absorbed by DNA[2,5-12].

49

50 The International Agency for Research on Cancer has classified broadband UVA (315-400nm) as
51 a Group 1 carcinogen, based on sufficient evidence for carcinogenicity in both humans and
52 experimental models combined with strong mechanistic considerations[13]. While UVA is found in
53 sunlight, most of UVA environmental toxicity has been attributed to the use of commercial
54 products, such as tanning beds[14]. Consistently, meta-analyses have shown a causal relation
55 between skin cancer and irradiation with UV-emitting tanning devices[13,15]. Further, it has been
56 demonstrated that skin squamous-cell carcinoma will develop in mice after long-term exposure to
57 broadband UVA[16-19]. Prior experimental studies have also suggested that UVA irradiation leads to
58 indirect DNA damage mostly through the accumulation of 8-oxo-7,8-dihydro-2′-deoxyguanosine
59 (8-oxo-dG) derived from reactive oxygen species[20-24]. Studies using reporter single-gene assays
60 have identified an enrichment of C:G>A:T mutations in UVA irradiated samples consistent with

61 damage due to 8-oxo-dG[25-28]. Despite prior evidence for carcinogenicity of broadband UVA (315-
62 400nm), UVA radiation in subsets of this spectrum is widely used in a surfeit of consumer products
63 without extensive evaluation of the potential carcinogenic and mutagenic effects of these products.
64 One prominent example is UV-nail polish dryers, which have become increasingly popular in the
65 last decade[29,30].
66
67 UV-nail lamps are used to cure and dry nail polish formulas, known as gels, which are oligomers
68 requiring exposure to UV radiation to harden into polymers. These UV-gel nail devices release
69 UVA radiation with either very little or, in most cases, no UVB radiation[31]. UV-gel nail devices
70 contain multiple bulbs, emitting UV wavelengths between 340 and 395nm that can react and
71 activate the photo-initiators in a gel[29]. Concerns have been raised regarding the magnitude of DNA
72 damage that can be posed from exposure to UV-nail machines and their potential role in skin
73 carcinogenesis[30,32]. Notably, in most cases, both nails and hands are irradiated up to 10 minutes
74 with a UV-nail dryer per session[32]. The number of nail salon clients is estimated to reach 8 clients
75 a day per nail technician, accounting for approximately 3 million daily clients in the United
76 States[33]. Typically, regular users change their gel manicures every 2 weeks[32]. Recently, a small
77 number of melanoma and non-melanoma cases, reported either on the nail or on the dorsum of the
78 hand, have also been putatively attributed to exposure to UV radiation emitted by nail polish
79 dryers[32,34].
80
81 To evaluate the DNA damage and mutagenic effects of ultraviolet radiation emitted by nail polish
82 UV-dryers on mammalian cells, we performed an *in vitro* irradiation of human and murine primary
83 cells using distinct acute and chronic exposure protocols. Irradiated and control cells were

84 subjected to multiple assays for measuring DNA damage as well as to DNA sequencing either by
85 bulk whole-genome sequencing after clonal expansion or by single-molecule duplex sequencing
86 without clonal expansion (**Figure 1**).
87

88 **RESULTS**

89 **Experimental Design and Examination of Cytotoxicity**

90 To study the cytotoxic effect of irradiation by a UV-nail polish dryer, mouse embryonic fibroblasts
91 (MEFs), human foreskin fibroblasts (HFFs), and adult human epidermal keratinocytes (HEKa)
92 were exposed under several distinct conditions (**Figure 1**). Each primary cell line was irradiated
93 one, two, or three times, with the duration of each exposure lasting between 0 and 20 minutes. Cell
94 viability was measured 48 hours after the final irradiation with each condition repeated at least
95 three times. Analysis of cell viability revealed that UV radiation induced cytotoxicity with higher
96 number of exposures causing a lower cell viability (**Figure 2*a***). For example, in all cell line
97 models, a single 20-minute irradiation resulted in 20% to 30% cell death, while three consecutive
98 20-minute exposures caused between 65% and 70% cell death (q-values < 0.05; Mann-Whitney U
99 tests; **Figure 2*a***).

100

101 Assessment of DNA damage was performed on MEFs and HFFs after either two 20-minute
102 irradiations taking place within 2 hours in a single day (termed, acute exposure; **Figure 1*a&c***) or
103 after three 20-minute irradiations each occurring in 3 consecutive days (termed, chronic exposure;
104 **Figure 1*a&c***). Assessment of DNA damage was also performed at the same timepoint for
105 unexposed MEF and HFF cells. Moreover, to assess the presence of somatic mutations, both
106 irradiated and control cells were subjected to barrier bypass-clonal expansion[35], grown for the
107 same number of doubling populations, and subjected to bulk whole-genome sequencing (**Figure**
108 **1*c***; **Supplemental Figure 1**). Specifically, irradiated and control MEF cells were grown for ~28
109 doubling populations prior to bulk whole-genome sequencing, while exposed and unexposed HFF
110 cells were grown for ~35 rounds of cell division (**Figure 1*c***; **Supplemental Figure 1**).

111 In the case of HEKa, cells were only chronically exposed with three 20-minute irradiations each
112 occurring in 3 consecutive days (**Figure 1*b***). Assessment of DNA damage in HFFs was conducted
113 similarly to the assessments perform for MEFs and HFFs (**Figure 1*c***). Nevertheless, somatic
114 mutations in HEKa cells were detected using an orthogonal approach to the one applied for MEFs
115 and HFFs by avoiding barrier bypass-clonal expansion. Specifically, irradiated and control HEKa
116 cells were grown for exactly 14 days, corresponding to approximately 8 doubling populations, and
117 were subsequently subjected to targeted single-molecule duplex sequencing[36].
118

119 **Quantification of Genotoxicity**

120 Genotoxicity of mammalian cells irradiated with a UV-nail polish dryer was evaluated 4 hours
121 after exposure using γH2Ax immunofluorescence[37]. Statistically significant increases in the
122 number of γH2Ax foci were observed when comparing irradiated MEF, HFF, and HEKa to control
123 cells for all cell lines as well as for all types of exposure (**Figure 2*b-e***). For MEFs, the number of
124 γH2Ax foci increased 186-fold for acute exposure when compared to control samples (q-value:
125 3.6×10^{-4}; Mann-Whitney U test) and 183.3-fold for chronic exposure (q-value: 2.5×10^{-4}; **Figure**
126 **2*c***). Acutely exposed HFFs had 154.7-fold elevation of the number of γH2Ax foci when compared
127 to control samples (q-value: 3.6×10^{-4}), while chronically exposed HFFs exhibited 137-fold
128 elevation (q-value: 1.2×10^{-5}; **Figure 2*d***). Similarly, irradiated HEKa cells showed a significant
129 increase of γH2Ax foci when compared to control samples with 398-fold elevation for acute
130 exposure (q-value: 3×10^{-9}) and 260-fold for chronic exposure (q-value: 2×10^{-9}; **Figure 2*e***).
131

132 **Evaluation of Photoproducts' Formation**

133 Immunofluorescence was used to evaluate whether irradiation from a UV-nail dryer resulted in the
134 formation of cyclobutane pyrimidine dimers (CPDs) or pyrimidine-pyrimidone (6-4) photoproduct

135 (6-4PPs) in all cell lines models after either acute or chronic exposure (**Supplementary Figure 2**).
136 As a positive control, each cell line model was also exposed to ultraviolet C light (UVC), which is
137 known to form these photoproducts[38]. Our results demonstrated that, in contrast to UVC radiation,
138 UV emitted by a nail-polish dryer induced neither CPDs nor 6-4PPs in any of the exposed cell
139 lines (**Supplementary Figure 2**).
140
141 **Quantification of Oxidative Damage**
142 To evaluate oxidative damage after irradiation, we utilized three independent *in vitro* assays,
143 including: *(i)* CellROX for detection of oxidative stress[39]; *(ii)* enzyme-linked immunosorbent assay
144 (ELISA) for quantification of 8-oxo-dG[40,41]; and *(iii)* OxiSelect™ for detection of cytosolic and
145 extra-cellular reactive oxygen species (ROS)[42].
146
147 CellROX green is a fluorogenic probe used for measuring oxidative stress in live cells, namely
148 superoxide radical anion ($O_2^{\bullet}$) and hydroxyl radical (•OH)[39]. The reduced state of the CellROX
149 dye is weakly fluorescent inside cells but once oxidized by ROS, the dye binds to nucleic acids in
150 cells and exhibits bright green photostable fluorescence[39]. The three cell models (MEF, HFF, and
151 HEKa) were tested using CellROX green dye immediately after irradiation (**Figure 1*c***). Live cell
152 imaging results unveiled a clear increase of CellROX green fluorescence in irradiated cells
153 compared to controls in all cases (**Figure 3*a-b***). To ensure that the CellROX fluorescence is due
154 to ROS formation in the cells, we further challenged the HEKa cells with a ROS scavenger, namely
155 N-acetyl-L-cysteine (NAC), prior to irradiation[43]. Quantification of the number of CellROX foci
156 without NAC treatment revealed a significant increase of oxidative stress in irradiated HEKa cells
157 when compared to the controls (5.5-fold increase for acute, q-value $< 2.2 \times 10^{-16}$; 4.4-fold increase

158 for chronic, q-value < 2.2 x 10^{-16}; Mann-Whitney U tests). Importantly, the number of CellROX
159 foci significantly decreased after NAC treatment when compared to untreated cells (acute: 5.2-
160 fold decrease, q-value= 2 x 10^{-3}; chronic: 4.2-fold decrease, q-value= 1.4 x 10^{-3}), confirming that
161 irradiation by a nail polish dryer is responsible for oxidative stress induction in mammalian cells.
162
163 ELISA quantifications of 8-oxo-dG were performed for all cell line modes in 3 distinct timepoints:
164 *(i)* immediately after exposure; *(ii)* 4 hours post-irradiation; and *(iii)* 24 hours post-irradiation
165 (**Figure 3*c-e***). Additionally, three positive controls, namely, hydrogen peroxide (H_2O_2), ultraviolet
166 C radiation (UVC), and potassium bromate ($KBrO_3$), were also evaluated for each of the cell lines
167 immediately after exposure (**Figure 3*c-e***). Overall, statistically significant enrichments of 8-oxo-
168 dG concentrations, ranging from 5- to 20-fold (q-values < 0.05), were observed in irradiated cells
169 when compared to the control cells for all cell line models and for all exposure types (**Figure 3*c-***
170 ***e***). In all cases, this level of enrichment was comparable or higher to the one exhibited by the
171 exposure to positive controls. Moreover, the amount of 8-oxo-dG remained stable even 24 hours
172 after irradiation (**Figure 3*c-e***). These results confirm that irradiation by a UV-nail polish dryer
173 causes high levels of oxidative stress mediated by ROS formation and subsequent oxidation of
174 DNA bases via 8-oxo-dG formation.
175
176 To further evaluate the total free radicals in the irradiated MEF and HFF cells, we utilized
177 OxiSelect™ *In Vitro* ROS/RNS Assay Kit. This assay employs a proprietary quenched fluorogenic
178 probe, dichlorodihydrofluorescin DiOxyQ (DCFH-DiOxyQ), which is newly developed derivative
179 of DCFDA and has been shown to be more specific for the detection of ROS/RNS[42,44,45]. Cytosolic
180 and extra-cellular ROS signals were evaluated in MEF and HFF samples, in three different

181 timepoints: *(i)* immediately after exposure, *(ii)* 20 minutes post-irradiation, and *(iii)* 24 hours post-
182 irradiation. (**Supplementary Figure 3**). ROS-induced florescence was elevated in both acutely
183 and chronically exposed mammalian cells compared to the untreated cells. For both MEFs and
184 HFFs, acute exposure resulted in 2- to 8-fold increase of both cytosolic and extra-cellular ROS
185 compared to their respective controls (q-values: 2×10^{-5} and 1.7×10^{-6} for MEF cytosolic and
186 extracellular, respectively; q-values: 2×10^{-3} and 3×10^{-5} for HFF cytosolic and extracellular,
187 respectively; Mann-Whitney U tests; **Supplementary Figure 3**).
188
189 **Examining Mitochondrial Membrane Potential and ROS Generation**
190 As mitochondria are particularly sensitive to excessive ROS generated by UV radiation and they
191 play key role in oxidants production[46,47], we also examined mitochondrial potential membrane and
192 evaluated the mitochondrial ROS production after irradiation with a UV-nail polish dryer.
193 Mitochondrial activity and functionality were conducted in all three cellular models 24 hours post-
194 irradiation by using a tetramethylrhodamine dye (TMRM), which is taken up by mitochondria with
195 a high proton gradient and is a measure of well coupled mitochondria (**Figure 4*a***; **Supplementary**
196 **Figure 4**). In all three cellular models, irradiation resulted in reduced TMRM fluorescence
197 indicating a likely mitochondrial loss of mitochondrial membrane potential (**Figure 4*a***;
198 **Supplementary Figure 4**). Moreover, MitoSOX red mitochondrial superoxide indicator dye was
199 applied to HEKa cells 24 hours post-radiation. MitoSOX selectively targets the mitochondria and,
200 after being oxidized by superoxide, it produces red fluorescence upon binding to nucleic acid in
201 the cells. Live cell imaging of acutely and chronically irradiated HEKa cells revealed MitoSOX
202 red fluorescence when compared to unexposed HEKa controls (**Figure 4*b***). Quantification of the
203 number of MitoSOX foci per cell revealed a significant increase of oxidative stress in mitochondria

204 of irradiated HEKa cells when compared to the controls (8.3-fold increase for acute, q-value: 7.4
205 x 10^{-12}; 17-fold increase for chronic, q-value < 3.6 x 10^{-10}; Mann-Whitney U tests; **Figure 4*c***).
206 This increase in MitoSOX fluorescence putatively suggests an elevation of oxidative stress in
207 mitochondria caused by irradiation. Taken altogether, these data suggest that UVA light can cause
208 mitochondrially generated ROS and persistent nuclear DNA damage.
209
210 **Somatic Mutations After Barrier Bypass-clonal Expansion**
211 To evaluate the somatic mutations engraved by UV radiation from a nail dryer, we utilized two
212 orthogonal sequencing approach: *(i)* bulk whole-genome sequencing of immortalized HFF and
213 MEF clones, grown for the same number of doubling populations after barrier bypass-clonal
214 expansion (**Supplementary Figure 1**); and *(ii)* single molecule duplex sequencing for HEKa cells
215 without clonal expansion (**Figure 1*b***). A total of 15 HFF and 15 MEF immortalized clones were
216 subjected to bulk whole-genome sequencing (WGS) at 30x coverage, including: *(i)* 5 HFF and 5
217 MEF clones after acute irradiation; *(ii)* 5 HFF and 5 MEF clones after chronic irradiation; *(iii)* 5
218 HFF and 5 MEF unirradiated control clones. Somatic mutations were derived for immortalized
219 clones by comparing the WGS data of each immortalized clone to the WGS data from the
220 respective primary cell line using previously established state-of-the-art bioinformatics pipelines
221 (**Figure 1**; **Supplementary Figure 5**). Examining the variant allele frequencies (VAFs) for single
222 base substitutions revealed that the majority of MEF mutations are subclonal with a mean VAF of
223 approximately 0.25, while most HFF mutations are clonal with a mean VAF of approximately 0.50
224 (**Supplementary Figure 6*a-b***). These results are consistent with previous observations in these
225 model systems[35,48] and they reflect experimental differences between the murine and human cell
226 line models after clonal expansion. Specifically, MEFs undergoing barrier-bypass clonal

227 expansion are most likely to yield two subclonal populations[35,48], while HFFs undergoing single-
228 cell subcloning have a high propensity for selecting a single clone[35].
229
230 Single base substitutions (SBSs) were 2- and 2.5-fold elevated in acutely and chronically irradiate
231 MEF cells, respectively, when compared to control cells (q-values<0.01; Mann-Whitney U tests;
232 **Figure 5*a***). Stratification of SBSs based on their simplest six channel classification (*i.e.*, C>A,
233 C>G, C>T, T>A, T>C, T>G; each mutation referred to by the pyrimidine base of the Watson-
234 Crick DNA base-pair) revealed a significant increase of C>A transversions in acute and chronic
235 MEFs exposed to UV emitted from a nail dryer: 2.8- and 4.2-fold increase for acute and chronic,
236 respectively (q-values: 0.02 and 0.016; Mann-Whitney U tests; **Figure 5*b***). Importantly, the
237 number of C>A single base substitutions found in MEF clones was positively correlated with the
238 number of UV exposures (**Figure 5*c***; Spearman correlation: 0.64; p-value*:* 0.0098).
239
240 Immortalized HFF clones exhibited similar behaviors to the ones of MEF clones, albeit, in most
241 cases, with smaller effect sizes. Specifically, substitutions were 1.2- and 1.4-fold enriched in
242 acutely and chronically irradiated HFF cells compared to control cells (q-values<0.01; Mann-
243 Whitney U tests; **Figure 5*a***). An elevation of C>A mutations was also observed in acutely
244 irradiated HFF clones (1.22-fold increase with q-value: 0.015; Mann-Whitney U tests; **Figure 5*b***)
245 as well as in chronically irradiated HFF clones (1.63-fold increase with q-value: 7.9×10^{-3}; Mann-
246 Whitney U tests; **Figure 5*b***). Similarly, the number of C>A transversions exhibited a positive
247 correlation with the number of UV exposures in HFFs (**Figure 5*c***; Spearman correlation: 0.85; p-
248 value*:* 5.9×10^{-5}). No differences in the numbers of small insertions or deletions were observed
249 between the irradiated and the control cells for any of the used cell line models (**Figure 5*d***).

250

251 **Somatic Mutations After Duplex Sequencing**

252 In principle, detection of somatic mutations in experimental systems requires clonal expansion[35]
253 and, for MEF and HFF cell lines, we utilized barrier bypass-clonal expansions prior to bulk whole-
254 genome sequencing. Recently, single-molecule duplex sequencing approaches have provided an
255 alternative high-fidelity protocol for directly measuring the mutagenic impact of genotoxic agents
256 without the need for clonal expansion, whilst improving the accuracy of NGS by more than 10,000-
257 fold and enabling sensitive detection of extremely rare mutations, such as those induced by
258 mutagens[36,49,50]. Importantly, duplex sequencing does not sequence a single cell or even a small
259 number of cells, rather, the method generally interrogates millions of double-stranded DNA
260 coming from many thousands of cells[51]. Thus, the mutational profile from duplex sequencing
261 provides an average somatic mutational profile across the complete population of exposed
262 cells[36,49,50].

263

264 We used a commercial targeted duplex sequencing protocol for assessing mutagenesis without
265 clonal expansion[36] both to provide an orthogonal validation of the previous results and to account
266 for any potential artifacts due to clonal expansion in MEF and HFF cell lines. Specifically, we
267 detected somatic mutations using duplex sequencing data from 3 chronically irradiated and 3
268 unirradiated control HEKa cells (**Method**). Similar to irradiated HFFs and MEFs, chronically
269 exposed HEKa exhibited 1.3-fold increase of substitutions when compared to control cells (**Figure**
270 **6*a***; q-value: 0.02; Mann-Whitney test). Importantly, C>A transversions were 2.2-fold enriched in
271 chronically irradiate HEKa cells compared to control cells (q-values: 0.04; Mann-Whitney tests;
272 **Figure 6*b***). Moreover, a positive correlation between the number of C>A transversion and the

273 number of UV exposures was also evident in HEKa cells (**Figure 6*c***; Spearman correlation: 0.88;
274 p-value: 0.021). Consistent with prior results, no changes were observed for small insertions or
275 deletions between irradiated and control HEKa cells (**Figure 6*d***).
276
277 **Mutational Signatures Engraved by Irradiating with a UV-nail Polish Dryer**
278 Previously, we have shown that different endogenous and exogenous mutational processes engrave
279 characteristic patterns of somatic mutations, termed, mutational signatures[52-54]. To evaluate the
280 mutational signatures engraved by irradiation with a UV-nail polish dryer, we performed separate
281 analysis of mutational signatures for MEFs, HFFs, and HEKa data. To explain the SBS patterns
282 of mutations observed in the irradiated cells, any known COSMIC signature[55] that improved the
283 reconstruction above the background models was allowed. For the analyses of MEF data, in
284 addition to known COSMIC signatures, we also allowed mouses specific mutational signatures
285 previously observed either *in vitro*[48] or *in vivo*[56] murine models (**Supplementary Figure 7*a***).
286
287 Our analyses revealed that only COSMIC signatures SBS18 and SBS36 (SBS18/36), both
288 previously attributed to reactive oxygen species[57,58], were found to be operative in all irradiated
289 MEF and HFF cells. It should be noted that ROS signatures SBS18 and SBS36 have cosine
290 similarity of 0.914 (**Figure 7*a***), which, in many cases, makes them hard to distinguish from one
291 another and these signatures are commonly reported together as SBS18/36[59-61]. Our analyses
292 revealed that SBS18/36 were the only signatures enriched in irradiated HFF and MEF samples
293 when compared to controls (**Figure 7*b-c***; q-values<0.05; Mann-Whitney tests). No other
294 mutational signature found in these samples was elevated in irradiated samples when compared to
295 control samples (**Supplementary Figure** 7***b&d***). Moreover, the identified sets of operative

296 mutational signatures allowed accurately reconstructing the mutational patterns in both MEFs and
297 HFFs (**Supplementary Figure** 7***c&e***).
298
299 Observing signatures SBS18/36, which are almost exclusively characterized by C>A substitutions
300 (**Figure 7*a***), in irradiated clones confirms that radiation emitted by a UV-nail polish dryer not only
301 oxidizes DNA but also results in permanently engraved patterns of C>A somatic mutations on the
302 genomes of irradiated cells. Similarly, an almost 3-fold enrichment of signatures SBS18/36 (p-
303 value < 0.0001; Fisher's exact test) was observed in keratinocytes irradiated with a UV-nail polish
304 dryer when compared to controls. Specifically, 65% of the mutations in UV-irradiated HEKa cells
305 were attributed to SBS18/36 (**Figure 7*d-e***), accounting for a total of 151 mutations
306 (**Supplementary Figure 7*f***). In contrast, in unirradiated control samples, SBS18/36 accounted for
307 23% of mutations (*i.e.*, 21 mutations; **Figure 7*d-e*; Supplementary Figure 7*f-g***).
308
309 Re-examination of the recently published set of 144 whole-genome sequenced skin cancers from
310 the Pan-Cancer Analysis of Whole Genomes (PCAWG) project[62] revealed a positive correlation
311 between C>A and C>T mutations (Pearson's correlation: 0.87; p-value < 2.2×10^{-16}; **Figure 7*f***).
312 Moreover, an average skin cancer appears to harbor approximately 2,500 C>A substitutions (95%
313 CI: 2,015 – 2,868) in their genome with 80% of their pattern attributed to signatures SBS18/36.
314 However, these C>A substitutions account for only 2.3% of the mutations observed in the 144
315 melanomas; 85% of mutations in these melanomas are generated by signature 7 – mutational
316 signature attributed to cyclobutane-pyrimidine dimers and 6-4 photoproducts from ultraviolet
317 light[62]. Importantly, 20 of the 169 substitutions (11.83%) identified as driver mutations[62] in these
318 samples can be attributed to signatures SBS18/36. This indicates that, while signatures SBS18/36

319 generate low numbers of mutations in skin cancer, they play an important role in generating
320 somatic mutations that contribute towards tumor development and cancer evolution.

321 **DISCUSSION**

322 In this report, we employed well-controlled experimental models for UV irradiation using a UV-
323 nail polish dryer and evaluated the DNA damage and mutagenic changes engraved on the genomes
324 of mammalian cells (**Figure 1**). The utilized *in vitro* clonal expansion models, MEFs and HFFs,
325 manifest the specific features required for mimicking human carcinogenesis and for recapitulating
326 the activity of characteristic mutational processes[35]. Both MEFs and HFFs underwent clonal
327 expansion after a barrier bypass step (senescence for MEFs and single-cell bottleneck for HFFs)
328 leading to the formation of exposure-derived clones, which were grown for the same number of
329 doubling populations (**Supplementary Figure 1**). As an orthogonal approach, we also utilized
330 HEKa primary cells, which cannot go through clonal expansion in culture. Cytotoxicity and
331 genotoxicity were observed in all irradiated cells; importantly, we observed an elevation of ROS
332 in irradiated cells leading to increased levels of 8-oxo-dG, which was confirmed by multiple *in*
333 *vitro* assays (**Figure 3**). Moreover, mitochondrial dysfunction was evident upon UVA radiation
334 (**Figure 4** and **Supplementary Figure 4**). Genomic profiling revealed higher levels of somatic
335 mutations in irradiated cells with C>A mutations being highly elevated in exposed samples
336 (**Figures 5** and **6**). Consistent with the increase of ROS, COSMIC signatures SBS18/36, two
337 mutational signatures previously attributed to reactive oxygen species[57,58], were engraved on the
338 genomes of irradiated samples and enriched in irradiated samples when compared to controls
339 (**Figure 7**).

340

341 Broadband UVA (315-420nm) has been extensively studied in the context of tanning devices and
342 classified as carcinogen by the International Agency for Research on Cancer[13]. Prior experimental
343 studies with broadband UVA have shown that it causes an accumulation of 8-oxo-dG[20-24],

344 generates C>A mutations in single-gene assays[25-28], and even induces tumors in mice[63]. Indeed,
345 prior studies have shown that UVA can generate low level of C>T somatic mutations consistent
346 with pyrimidine-pyrimidine photodimers[64]. Intriguingly, in this study, we demonstrate that UVA
347 with wavelengths between 365 and 395nm, which is generally considered to be safe and is
348 commonly used in a plethora of consumer products, causes DNA oxidative damage leading to
349 C>A mutations; no evidence was found that radiation generated by the UV-nail polish machine
350 generates any pyrimidine-pyrimidine photodimers (**Supplementary Figure 2**).
351
352 Our findings are also consistent with prior cancer epidemiological observations. In principle, males
353 have significantly higher risk than females to develop melanoma[65,66]. Surprisingly, this trend is
354 reversed when one examines cancer risk in melanomas of the hand in younger women.
355 Specifically, young females (ages 15 to 39) have approximately 2-fold higher risk for developing
356 melanoma of the upper extremities compared to young males[67]. This higher risk is possibly due to
357 lifestyle choices, one of which may be radiation from consumer products such as UV-nail polish
358 dryers[67]. It should be noted that exposure to UV-light from the sun cannot reasonably explain the
359 higher risk in young females as there is no observed differences in melanoma risk between young
360 males and females for other parts of the body commonly exposed to the sunlight, *viz.*, face, head,
361 and neck[66,67].
362
363 While this report demonstrates that radiation from UV-nail polish dryers is cytotoxic, genotoxic,
364 and mutagenic, it does not provide direct evidence for increased cancer risk in human beings. Prior
365 studies have shown that an increase in mutagenesis will likely lead to an increase in cancer risk[68-
366 70]. Further, several anecdotal cases have demonstrated that cancers of the hand are likely due to

367 radiation from UV-nail polish dryers[32,34]. Taken together, our experimental results and the prior
368 evidence strongly suggest that radiation emitted by UV-nail polish dryers may cause cancers of
369 the hand and that UV-nail polish dryers, similar to tanning beds[71], may increase the risk of early-
370 onset skin cancer[72]. Nevertheless, future large-scale epidemiological studies are warranted to
371 accurately quantify the risk for skin cancer of the hand in people regularly using UV-nail polish
372 dryers. It is likely that such studies will take at least a decade to complete and to subsequently
373 inform the general public. In the meantime, this report aims to raise awareness of the likely cancer-
374 causing role of artificial UV lamps and caution people who regularly use UV-nail polish dryers.

375 **MATERIALS AND METHODS**

376 **UV-nail polish machine characteristics**

377 A 54-Watt UV nail drying machine was purchased (model: MelodySusie), harboring 6 bulbs that
378 emit UV photons for curing gel nail polish. Based on the manufacturer's specifications, the UV
379 nail drying machine emits ultraviolet A light in wavelengths between 365 and 395nm. The UV
380 power density was evaluated using a UV513AB Digital UVA/UVB Meter that can measure UV
381 radiation between 280 and 400 nm. The machine stabilizes at ~7.5 mW/cm^2, within minutes
382 (**Supplementary Figure 8*a-b*),** putting it on the lower end of the power density spectrum
383 calculated for commonly used UV-nail machines[31] (median of 10.6 mW/cm^2). In this study, in
384 most cases, we performed a 20-minute UV exposure session which is equivalent to a total amount
385 of energy delivered per unit area of 9 J/cm^2:

386

387 $$7.5\ mW/cm^2 * 20\ minutes = 7.5\ mJ/(sec*cm^2) * 1200\ sec = 9000\ mJ/cm^2 = 9\ J/cm^2$$

388

389 **Cell culture, irradiation, and immortalization of mouse embryonic fibroblasts (MEFs)**

390 Primary mouse embryonic fibroblasts (MEFs) were expanded in Advanced DMEM supplemented
391 with 15% fetal bovine serum, 1% penicillin/streptomycin, 1% sodium pyruvate and 1% glutamine,
392 and incubated in 20% O_2 and 5% CO_2. At passage 2, the primary cells were seeded in six-well
393 plates for 24 hours, until adherence, then exposed for 20 minutes to the UV-nail machine in pre-
394 warmed sterile PBS. Control cells were kept in PBS for 20 minutes. Cells were irradiated with a
395 UV nail polish dryer, acutely (*i.e.*, twice a day, with 60 minutes break between each of the 2
396 sessions) as well as chronically (*i.e.*, once every day for up to 3 consecutive days). At the end of
397 every irradiation, the cells were washed, and complete pre-warmed medium was replenished.

398 Exposed and control primary cells were cultivated until bypassed a barrier step through
399 senescence. Upon barrier bypass, the cells reached clonal expansion allowing the isolation of *bona*
400 *fide* cell clones (**Supplementary Figure 1*a***). In all cases, irradiated and control MEF cells were
401 grown for ~28 doubling populations prior to bulk whole-genome sequencing. Fifteen clonally
402 expanded populations were successfully isolated and subjected to bulk whole-genome sequencing,
403 including: 5 replicates acute exposure, 5 replicates of chronic exposure, and 5 replicates for
404 unirradiated control cells. All cell cultures were routinely tested for the absence of mycoplasma.
405
406 **Cell culture, irradiation, and immortalization of human foreskin fibroblasts (HFFs)**
407 Primary human cells derived from human foreskin fibroblasts (HFFs) were provided to us by Dr.
408 John Murray (Indiana University Bloomington). Early passage cells were expanded in Advanced
409 DMEM supplemented with 10% fetal bovine serum and 1% glutamine in 5% CO_2 incubator.
410 Irradiation with a UV-nail polish dryer followed the same protocol as the one for MEFs (**Figure**
411 **1*a***). Similarly, control HFF cells were kept in PBS for 20 minutes during all irradiations. Clonal
412 expansion was carried out using serial dilutions procedure in 96-well plates, assuming 30%
413 probability of a single-cell clone formation per well (**Supplementary Figure 1*b***). Wells were
414 washed weekly, until clones reached confluency and were transferred progressively to T-75 flasks.
415 In all cases, irradiated and control HFF cells were grown for ~35 rounds of cell division. Fifteen
416 clonally expanded populations were successfully isolated and subjected to bulk whole-genome
417 sequencing, including: 5 replicates acute exposure, 5 replicates of chronic exposure, and 5
418 replicates for unirradiated control cells. All cell cultures were routinely tested for the absence of
419 mycoplasma.
420

421 **Cell culture and irradiation of adult human epidermal keratinocytes (HEKa)**

422 Primary human keratinocytes, derived from normal adult human epidermal keratinocytes (HEKa),
423 were purchased from ATCC (PCS-200-011; Lot number: 70033063). Early passage cells were
424 expanded in Dermal Cell Basal Medium (PCS-200-030) supplemented with Keratinocyte Growth
425 Kit (PCS-200-040) and antibiotics (Penicillin: 10 Units/mL, Streptomycin: 10 µg/mL,
426 Amphotericin B: 25 ng/mL) in 5% CO_2 incubator. At passage 2, the primary cells were seeded at
427 a density of 2.5 x 10^3 cells/cm^2 in 10-cm dishes for 24 hours. Subsequently, cells were only
428 chronically irradiated with a UV-nail polish dryer following the same protocol as the for MEFs
429 and HFFs (**Figure 1*b*)**. Similarly, control HEKa cells were kept in PBS for 20 minutes during all
430 irradiations. In all cases, irradiated and control HEKa cells were grown for exactly 14 days,
431 corresponding to approximately 8 rounds of cell division, which allows sufficient time for DNA
432 adduct/damage to be fixed as somatic mutation(s) but not enough time to result in a clonal
433 expansion[36]. Unexposed cells were grown for the same duration as irradiated cells. Six cell
434 populations were successfully isolated and subjected to subjected to duplex sequencing, including:
435 3 replicates for chronic exposure and 3 replicates for unirradiated control cells. All cell cultures
436 were routinely tested for the absence of mycoplasma.

437

438 **Cell viability and cytotoxicity assays**

439 Primary cells were seeded in 24-well plates and exposed to the UV drying device as indicated.
440 Cell viability was measured 48 hours after treatment cessation using the Cell-Counting Kit 8
441 (CCK-8) from Dojindo. Plates were incubated for 3 hours at 37°C and absorbance was measured
442 at 450 nm using the Infinite 200 Tecan *i*-control plate reader machine. The CCK-8 assay was
443 performed in at least 4 replicates for each experimental condition. Trypan Blue exclusion assay

444 was also performed for assessing cell viability upon exposure, validating the choice for selecting
445 the irradiation condition that causes around 50% cell death (**Supplementary Figure 8*c*)**.
446
447 **Assessment of genotoxicity using γH2Ax immunofluorescence**
448 Immunofluorescence staining was carried out using a monoclonal antibody specific for Ser139-
449 phosphorylated H2Ax (γH2Ax) (9718, Cell Signaling Technology). Briefly, primary cells were
450 seeded on coverslips in 24-well plates and, the following day, irradiated in triplicates as previously
451 described. Four hours after treatment cessation, the cells were fixed with 4% formaldehyde at room
452 temperature for 15 minutes, followed by blocking in 5% normal goat serum (5425, Life
453 Technologies) for 60 minutes. Subsequently, the cells were incubated with γH2Ax-antibody (1:400
454 in 1% BSA) at 4°C, overnight. A fluorochrome-conjugated anti-rabbit secondary antibody (4412,
455 Cell Signaling Technology) was then incubated for 1 hour at room temperature. ß-actin staining
456 was followed using phalloidin (8953, Cell Signaling Technology) incubated for 15 minutes at
457 room temperature. Coverslips were mounted in ProLong Gold Antifade Reagent with DAPI (8961,
458 Cell Signaling Technology), overnight. Immunofluorescence images were captured using a
459 Confocal Laser Scanning Biological Microscope Olympus FV1000 Fluoview. Quantification of
460 γH2Ax fluorescent cells was computed using Fiji software.
461
462 **Investigation of photoproducts using CPD and 6-4PP immunofluorescence**
463 Immunofluorescence staining was carried out using anti-cyclobutane pyrimidine dimers (CPDs)
464 monoclonal antibodies (clone KTM53, Kamiya Biomedical) and anti-6-4 photoproducts
465 monoclonal antibodies (Clone 64M-2, Cosmo Bio). Briefly, primary cells were seeded on
466 coverslips in 24-well plates and, the following day, irradiated in triplicates as previously described.

467 Subsequently, the cells were washed with ice-cold CSK buffer, containing 100mM NaCl, 300mM
468 Glucose, 10mM PIPES, 3mM MgCl2 and 0.5% Triton, then fixed with 4% formaldehyde at room
469 temperature (RT) for 15 minutes, followed by permeabilization using 0.5% Triton for 5 minutes
470 on ice. DNase I treatment was performed to denaturalize the genomic DNA in the cells using 20U
471 DNase I for 40s per coverslip (NEB; DNase I (RNase-free), M0303S). For blocking, we used 1%
472 BSA (A3059, Sigma) and 5% normal goat serum (5425, Life Technologies) for 60 minutes.
473 Afterwards, the cells were incubated with the monoclonal antibodies (1:50 in 1% BSA) at 4°C,
474 overnight. A fluorochrome-conjugated anti-mouse Alexa Fluor 594 secondary antibody (8890S,
475 Cell Signaling Technology) was then incubated for 1 hour at room temperature. Coverslips were
476 mounted in ProLong Gold Antifade Reagent with DAPI (8961, Cell Signaling Technology),
477 overnight. Immunofluorescence images were captured using Nikon A1R-STORM Super
478 Resolution Microscope.
479
480 **Quantification of reactive oxygen species via CellROX**
481 Oxidative stress induces the production of reactive oxygen species (ROS) and reactive nitrogen
482 species (RNS) in cells. We employed the CellROX™ Green Reagent for detection of oxidative
483 stress (ThermoFisher Scientific; catalog number: C10444), immediately after irradiation. MEF,
484 HFF, and HEKa primary cells were seeded on Mattek 35-mm dishes from (P35G-1.5-14-C)
485 appropriate for high quality live cell imaging. CellROX green was added in pre-warmed complete
486 media to a final concentration of 5μM and incubated for 30 minutes at 37 ºC. CellROX solution
487 was washed carefully 3 times with pre-warmed PBS and normal media was replenished. Live cell
488 imaging was conducted using Nikon A1R-STORM Super Resolution Microscope. To ensure
489 CellROX selectivity towards ROS components, cells were challenged with 2mM N-acetyl-L-

490 cysteine (NAC) for 1 hour prior to UVA exposure. NAC is a known ROS scavenger. After
491 CellROX addition, live cell images were used for quantification of CellROX foci number, with
492 and without NAC pre-treatment, using General Analysis pipeline on Nikon WorkStation 5317.
493
494 **Quantification of reactive oxygen species via OxiSelect**
495 Additionally, we also utilized the OxiSelect™ *In Vitro* ROS/RNS Assay Kit (Green Fluorescence),
496 from Cell Biolabs, to evaluate the level of oxidative damage induced after irradiation, intra- and
497 extra-cellularly, immediately after exposure as well as 20 minutes and 1 day after irradiation.
498 Primary MEFs and HFFs were irradiated in triplicates in a 6-well plate, twice a day (acute
499 exposure) and once every day for 3 consecutive days (chronic exposure). PBS solutions were
500 collected immediately after the last UV treatments. After every treatment, the cells were washed
501 with pre-warmed PBS and complete media was replenished for the accounted waiting timepoints.
502 Thereafter, media solutions were collected 20 minutes and 24 hours after treatment cessation.
503 These solutions were used to assess extracellular ROS signals. Cytosolic ROS production was
504 evaluated after trypsinization of the cells, lysis of cellular membrane with 0.5% TritonX-100 and
505 centrifugation for 5 minutes at 10,000 rpm. Samples were loaded into a 96 black well plate,
506 together with varying concentrations of hydrogen peroxide for generating the standard curve, and
507 fluorescence signals were recorded using the Infinite 200 Tecan *i*-control plate reader machine at
508 480 nm excitation / 530 nm emission.
509
510 **Quantification of 8-hydroxy-2'-deoxyguanosine via ELISA**
511 We quantified 8-hydroxy-2'-deoxyguanosine (8-oxo-dG) for oxidative DNA damage in DNA
512 samples using the EpiQuik™ 8-OHdG DNA Damage Quantification Direct Kit (Colorimetric)

513 from Epigentek following manufacturer instructions. Briefly, primary MEF, HFF, and HEKa
514 primary cells were seeded on 10-cm dishes overnight. Three positive control exposures were
515 employed, after concentration optimization, namely 400μM H_2O_2 for 1 hour, 20J/m^2 UVC, and
516 4mM $KBrO_3$ for 1 hour. Following irradiation with nail polish dryer, cells were collected at the
517 selected timepoints (immediately, 4 hours, and 24 hours after irradiation) and subjected to genomic
518 DNA extraction. Following Qubit DNA quantification, 300ng of DNA was loaded into strip wells
519 that are specifically treated to have a high DNA affinity. 8-oxo-dG was detected using capture and
520 detection antibodies. The detected signal is enhanced, and the readout was measured at 450 nm
521 absorbance using the Infinite 200 Tecan *i*-control plate reader machine.
522
523 **Evaluation of mitochondrial ROS production and membrane potential**
524 Image-iT™ TMRM Reagent, and MitoSOX™ Red Mitochondrial Superoxide Indicator
525 (ThermoFisher Scientific; catalog number: I34361 and M36008, respectively), are two dyes that
526 target mitochondria in live cells, the former localizing active mitochondria with normal
527 mitochondria membrane potential, and the latter with affinity to ROS production. MitoTracker™
528 Green FM (ThermoFisher Scientific, catalog number: M7514) was utilized to localize
529 mitochondria regardless of mitochondrial membrane potential. Briefly, primary cells were seeded
530 on Mattek 35-mm dishes (P35G-1.5-14-C) overnight and incubated for 30 minutes in pre-warmed
531 live imaging staining solution (ThermoFisher Scientific, catalog number: A14291DJ) containing
532 100μM MitoTracker reagent. TMRM dye was added in pre-warmed Live Imagining Solution to a
533 final concentration of 100nM and incubated for 30 minutes at 37 ºC. MitoSOX solution was
534 prepared in pre-warmed Live Imagining Solution to a final concentration of 200nM and incubated
535 for 10 minutes at 37 ºC. All solutions were washed carefully 3 times with pre-warmed PBS and

536 normal media was replenished. Live cell imaging was conducted using Nikon A1R-STORM Super
537 Resolution Microscope. Fluorescence data quantification was carried out using General Analysis
538 pipeline on Nikon WorkStation 5317.
539
540 **DNA extraction and bulk whole-genome sequencing**
541 Genomic DNA from MEF and HFF primary cells and immortalized clones were extracted using
542 Qiagen DNeasy Blood & Tissue kit, following the manufacturer instructions. Quality and quantity
543 of DNA were checked using NanoDrop and Qubit instruments. Around 2ug of DNA was thereby
544 extracted per each sample. High-quality DNA for 32 samples were sent to Novogene for whole-
545 genome library preparation and whole-genome sequencing at 30x coverage using paired-end 150
546 base-pair run mode with Illumina's HiSeq-XTen. The 32 samples included: *(i)* one primary HFF
547 and one primary MEF used as normal samples in the mutation calling; *(ii)* 5 HFF and 5 MEF
548 immortalized clones after acute irradiation; *(iii)* 5 HFF and 5 MEF immortalized clones after
549 chronic irradiation; and *(iv)* 5 HFF and 5 MEF unirradiated immortalized control clones.
550
551 **Identification of somatic mutations from whole-genome bulk sequencing**
552 FASTQ files were subjected to BWA-MEM alignment using GRCm38 and GRCh38 as reference
553 genomes for MEF and HFF, respectively. Our methodology for identification of somatic mutations
554 from bulk sequencing data follows established approaches from large genomics consortia[73,74].
555 Briefly, ensemble variant calling of somatic mutations was performed using three independent
556 variant callers Mutect2[75], VarScan2[76], Strelka2[77], and MuSe[78]. Any mutation identified by at least
557 two out of the four variant callers was considered a *bona fide* mutation. *Bona fide* mutations were
558 subsequently filtered to remove any residual SNPs based on dbSNP annotation by variant effect

559 predictor[79]. Further, any mutations shared between two or more samples and clustered mutations
560 were removed as these reflect either residual germline mutations or mutations under positive
561 selection (**Supplementary Figure 5**). Overall, a total of 118,429 unique somatic mutations were
562 detected across all sequenced samples prior to filtering. Consistent with prior datasets[73,74], the
563 germline filtering removed 18.7% of these mutations with another 5.2% removed by the clustered
564 filter. The remaining set of somatic mutations were used in the subsequent analyses and the
565 evaluation for mutational signatures.
566
567 **DNA extraction and duplex sequencing**
568 Genomic DNA from HEKa cells were extracted using Qiagen DNeasy Blood & Tissue kit,
569 following manufacturer instructions, with one exception during the initial proteinaseK digestion
570 for which the samples were incubated at 37℃ rather than 54℃ for 1 hour, and DNA yield was
571 eluted in IDTE buffer (10mM Tris HCl pH 8.0 + 0.1mM EDTA). Quality and quantity of DNA
572 were checked using NanoDrop and Qubit instruments. High-quality DNA for 7 samples were sent
573 to TwinStrand Biosciences for targeted library preparation, targeted duplex sequencing, and data
574 analysis. The seven samples included: *(i)* one primary HEKa sample used in the mutation calling;
575 *(ii)* 3 HEKa samples after chronic irradiation; and *(iii)* 3 HEKa unirradiated immortalized control
576 clones. Briefly, duplex library preparation was performed using a human mutagenesis panel (~50
577 kb distributed across the whole genome in regions not predicted to be under positive or negative
578 selection) on DNA input sufficient to generate between 500 million to 1 billion informative Duplex
579 base pairs per sample. Each sample was prepared in two batches: one with the standard
580 mutagenesis assay and one with a prototype rapid workflow version of the assay. All libraries were
581 sequenced on an Illumina NovaSeq 6000.

582

583

584

585 **Identification of somatic mutations from duplex sequencing**

586 All raw NovaSeq sequencing FASTQ data was processed through the TwinStrand cloud-based
587 human mutagenesis pipeline to generate error-corrected BAM files and variant call files for each
588 sample. Mutagenesis analysis was carried out using the *Min* assumption for mutant frequency
589 calculation as standardly done[36]. This method counts each variant only once, regardless of the
590 number of reads that contain the non-reference allele.

591 $$Mutant\ Frequency = \frac{\text{Number of Unique Variants}}{\text{Total non N Duplex Bases}}$$

592 The remaining set of somatic mutations were used in the subsequent analyses and evaluation for
593 mutational signatures.

Duplex sequencing yield results

Average raw reads per sample	**~239 million**
Average duplex bases per sample	**~982 million**
Average mean on target duplex depth	**15,204x**
Interspecies contamination	**Negative**
Inter-sample contamination	**Negative**
Hybrid selection efficacy	**~99.81%**
Variants VAF used	**≤ 1%**

594

595 **Analysis of mutational signatures and additional examinations**

596 Analysis of mutational signatures was performed using our previously derived set of reference
597 mutational signatures[55] as well as our previously established methodology with the SigProfiler
598 suite of tools used for summarization, simulation, visualization, and assignment of mutational
599 signatures[62,80,81]. Variant allele frequencies (VAF) were calculated using integrative genomics

viewer[82]. R version 3.6.1 was used to plot data (*i.e.,* ggplot2, easyGgplot2, ComplexHeatmap[83], and circlize[84] packages), to compute p-values (ggpubr package), to perform correlation analyses (corrr package), and to compute the cosine similarity (lsa[85] package).

604 **FIGURE LEGENDS**

605 **Figure 1. Overview of the overall study design.** ***(a)*** Primary mammalian cells, MEFs and HFFs,
606 were expanded into 6-well plates and treated with ultraviolet light (UV) emitted from a UV-nail
607 polish dryer for 20 minutes, twice a day within one single day, termed *acute UV exposure*. For
608 *chronic UV exposure*, primary cells were exposed consecutively in three different days with each
609 exposure lasting 20 minutes. Control samples were maintained in the dark in pre-warmed PBS for
610 20 minutes during each exposure session. After recovery and cellular selection, whether through
611 senescence bypass or single-cell subcloning, control and irradiated cell were grown for the same
612 number of doubling populations and subjected to bulk whole-genome sequencing. Analysis of
613 whole-genome sequenced samples was performed using our established pipelines for mutation
614 calling. Analysis of mutational signatures was performed using the SigProfiler suite of tools. ***(b)***
615 Primary HEKa cells were irradiated in 10-cm dishes using UV-nail polish dryer for 20 minutes for
616 three consecutive days. Control samples were maintained in the dark in pre-warmed PBS for 20
617 minutes during each exposure session. HEKa cells were kept in culture for recovery and
618 replication, allowing around 8 doubling-populations after which the cells were subjected to high
619 coverage duplex Sequencing. Analysis of duplex sequencing samples was performed using
620 commercially established pipelines. Analysis of mutational signatures was performed using the
621 SigProfiler suite of tools. ***(c)*** Asterisks in panels *(a)* and *(b)* denote timepoints when DNA damage
622 and other assessments were performed for each condition, including interrogation of cytotoxicity,
623 genotoxicity, oxidative damage, and mitochondrial damage.

624

625 **Figure 2. Cytotoxicity and genotoxicity in mammalian cells after irradiation with a UV-nail**
626 **dryer.** ***(a)*** Cytotoxicity assessment following exposure of primary MEFs (top panel), HFFs

627 (middle panel), and HEKa (bottom panel) to UV radiation emitted from a UV-nail polish dryer for
628 different timepoints, ranging from 0 to 20 minutes. Multiple UV-exposure sessions were tested
629 with one hour difference between each consecutive exposure, including: grey – one exposure in a
630 day; yellow – two exposures in a day; red – three exposures in a day. Formazan dye absorbance
631 was measured 48 hours after treatment cessation and was normalized to the number of unirradiated
632 control cells at timepoint 0. The results are presented as mean percentage ± standard deviation
633 from at least four replicates. ***(b)*** DNA damage evaluation by immunofluorescence of Ser139-
634 pjosphorylated histone H2Ax (γH2Ax). Primary MEFs (top panel), HFFs (middle panel) and
635 HEKa (bottom panel), were exposed to UV radiation either acutely or chronically. DAPI is shown
636 in blue, Phalloidin in red, and γH2Ax in green. ***(c-e)*** Quantification of the number of γH2Ax foci
637 was performed by analyzing at least 100 cells per condition, collected from at least triplicates, in
638 MEF ***(c)***, HFF ***(d)*** and HEKa ***(e)*** cells. Statically significant results from FDR corrected Mann-
639 Whitney U tests are denoted as: ***q-value<0.001 and ****q-value<0.0001.
640
641 **Figure 3. Oxidative damage in mammalian cells after irradiation with a UV-nail dryer. (*a*)**
642 Assessment of oxidative DNA damage by live imaging of CellROX green reagent in control and
643 irradiated MEF (top panel), HFF (middle panel), and HEKa (bottom panel) cells. DAPI is shown
644 in blue while CellROX is shown in green. ***(b)*** HEKa cells were challenged with 2mM N-acetyl-L-
645 cysteine (NAC) for 1 hour prior to irradiation. Quantification of the number of CellROX foci was
646 performed by analyzing at least 100 cells per condition and comparing cells with and without NAC
647 pre-treatment, collected from triplicates. Statically significant results from FDR corrected Mann-
648 Whitney U tests are denoted as: ***q-value<0.001 and ****q-value<0.0001. ***(c-e)*** Oxidative
649 DNA damage measurement of 8-oxo-dG by ELISA in MEF ***(c)***, HFF ***(d)***, and HEKa ***(e)*** cells.

650 Measurements of 8-oxo-dG were performed at different timepoints (0, 4, 24 hours post-treatment).
651 Measurements of 8-oxo-dG were also performed on a negative control (NC), consisting of water
652 only, and on three positive controls, namely, hydrogen peroxide (H_2O_2), ultraviolet C radiation
653 (UVC), and potassium bromate ($KBrO_3$). Statically significant results from FDR corrected Student
654 t-tests are denoted as: *q-value<0.05; *q-value<0.01; ***q-value<0.001; and ****q-
655 value<0.0001.
656
657 **Figure 4. Mitochondrial disruption after irradiation with a UV-nail dryer in HEKa cells.** ***(a)***
658 Evaluating the mitochondrial membrane potential after irradiation of HEKa cells with a UV-nail
659 dryer. DAPI is shown in blue, MitoTracker in green, and tetramethylrhodamine dye (TMRM) in
660 red. Yellow corresponds to overlaps between MitoTracker and TMRM. ***(b)*** Examining
661 mitochondrial ROS production in HEKa cells. DAPI is shown in blue, MitoTracker in green, and
662 MitoSOX in red. Yellow corresponds to overlaps between MitoTracker and MitoSOX. In both
663 panels (*a*) and (*b*), MitoTracker green reagent is used to localize mitochondria regardless of
664 mitochondria membrane potential. **(*c*)** Quantification of the number of MitoSOX foci in at least
665 100 cells per condition in HEKa, collected from at least triplicates. Statically significant results
666 from FDR corrected Mann-Whitney U tests are denoted as: ***q-value<0.001 and ****q-
667 value<0.0001.
668
669 **Figure 5. Mutations found in the genomes of MEFs and HFFs irradiated by a UV-nail dryer.**
670 ***(a)*** Mutation count per megabase (Mb) detected in the different conditions, represented in colors,
671 in MEFs and HFFs. ***(b)*** Fold-increase of single base substitutions in UV-treated clones compared
672 to controls. Fold increase is expressed as mean fold-change ± SE (standard error). ***(c)*** Spearman's

673 correlations between the number of C>A substitutions and the number UV exposures in the five
674 independent UV-treated clones. Acute and chronic exposures correspond to 2 and 3 exposures,
675 respectively. ***(d)*** Number of small insertions and deletions (indels) in MEF and HFF clones for
676 each irradiation condition. *: q-value<0.05; **: q-value<0.01; ***: q-value<0.001; ****: q-
677 value<0.0001.
678
679 **Figure 6. Mutation analysis of HEKa cells irradiated by a UV-nail dryer.** ***(a)*** Mutation count
680 per megabase (Mb) detected in the different conditions, represented in colors, in MEFs and HFFs.
681 **(*b*)** Fold-increase of single base substitutions in UV-treated clones compared to controls. Fold
682 increase is expressed as mean fold-change ± SE (standard error). ***(c)*** Spearman's correlations
683 between the number of C>A substitutions and the number UV exposures in each of the 3 biological
684 replicates. ***(d)*** Number of small insertions and deletions (indels) in HEKa cells.
685
686 **Figure 7. Somatic Mutations due to SBS18 in cells and PCAWG samples.** **(*a*)** Mutational
687 signatures COSMIC SBS18 and COSMIC SBS36 observed in UV irradiated cells. **(*b*)** Number of
688 mutations per megabase attributed to COSMIC SBS18/36 in UV exposed MEF clones, per
689 condition, *i.e.*, control (n=3/5), chronic (n=5/5), and acute (n=5/5) exposure. **(*c*)** Number of
690 mutation per megabase attributed to COSMIC SBS18/36 in UV exposed HFF clones, per
691 condition, *i.e.*, control (n=3/5), chronic (n=5/5), and acute (n=5/5) exposure. **(*d*)** Mutational
692 patterns of irradiated (upper track) and control (lower track) primary HEKa cells. **(*e*)** COSMIC
693 signatures assignment of UV-irradiated HEKa cells (upper track) and control (lower track). **(*f*)**
694 Correlation analysis of C>A and C>T mutations in 144 PCAWG skin cancer samples. **(*g*)**
695 Percentage contribution of the C>A mutations to SBS18/36 in PCAWGS skin cancer samples.
696

697 **SUPPLEMENTARY FIGURE LEGENDS**

698 **Supplementary Figure 1. Exposure and barrier bypass-clonal expansion assays.** ***(a)*** MEFs
699 were treated at early passages and led through senescence manifested by a plateau-like curve where
700 cells lost the ability to efficiently duplicate and grow. Cells went through senescence bypass and
701 eventually emerge into immortalized clones, able to multiply indefinitely, a process called barrier-
702 bypass clonal expansion, emulating oncogenesis. Irradiated and control MEF cells were grown for
703 ~28 doubling populations prior to bulk whole-genome sequencing (WGS). Exemplars are provided
704 for one control, one acutely irradiated, and one chronically irradiated MEF. Y-axes reflect the
705 number of doubling populations, while X-axes correspond to the number of days in culture. ***(b)***
706 HFFs were treated at early passages and led through recovery phase before initiating a single cell
707 subcloning assay using a serial dilutions technic. *Bona fide* single-cell clones were collected at the
708 end of experiment. Irradiated and control HEF cells were grown for ~35 doubling populations
709 prior to bulk whole-genome sequencing (WGS). Exemplars are provided for one control, one
710 acutely irradiated, and one chronically irradiated HFF. Y-axes reflect the number of doubling
711 populations, while X-axes correspond to the number of days in culture.

712

713 **Supplementary Figure 2. Evaluation of cyclobutane pyrimidine dimers and 6-4**
714 **photoproducts irradiated by a UV-nail dryer.** ***(a-c)*** Immunofluorescence of cyclobutane
715 pyrimidine dimers (CPDs) and 6-4 photoproducts (6-4PPs) in MEF ***(a)***, HFF ***(b)***, and HEKa ***(c)***
716 cells after acute or chronic irradiation with a UV-nail dryer. DAPI is shown in blue while CPDs
717 and 6-4PPs are shown in red. A positive control, namely, cells irradiated with ultraviolet C (UVC)
718 light (1x 10J/m^2), is also provided for each cell line.

719

720 **Supplementary Figure 3. Cytosolic and extra-cellular measurement of reactive oxygen**
721 **species in MEFs and HFFs.** Accumulation of reactive oxygen species (ROS) through time in
722 primary MEFs (left panel) and HFFs (right panel) after acute or chronic irradiation with a UV-nail
723 dryer. Each circle corresponds to a single experiment for a particular exposure. All y-axes reflect,
724 either cytosolic or extracellular, relative ROS fluorescence by normalizing the fluorescence of a
725 particular exposure to the average fluorescence of the appropriate controls. Statically significant
726 results from FDR corrected Mann-Whitney U tests are denoted as: ***q-value<0.001 and ****q-
727 value<0.0001.
728
729 **Supplementary Figure 4. Mitochondrial membrane potential after irradiation with a UV-**
730 **nail dryer.** Evaluating the mitochondrial membrane potential after irradiation of MEF cells ***(a)***
731 and HFF cells ***(b)*** with a UV-nail dryer. DAPI is shown in blue, MitoTracker in green, and
732 tetramethylrhodamine dye (TMRM) in red. Yellow corresponds to overlaps between MitoTracker
733 and TMRM.
734
735 **Supplementary Figure 5. Schematic of whole-genome data analysis.** Primary cells were
736 sequenced and used as a germline reference. We employed three variant callers (Mutect2,
737 VarScan2, Strelka2, and MuSe) in matched tumor-normal mode, with the primary cells' BAM
738 files as normal for each cell line. We selected variants called in at least 2 of the variant callers in
739 order to increase variant calling quality. Germline single nucleotide polymorphisms (SNP) were
740 removed using the dbSNP database. Any clustered mutation as well as any mutation observed in
741 2 or more samples were also removed. The final set of somatic mutations were analyzed by the
742 SigProfiler suite of tools.

743 **Supplementary Figure 6. Analysis of variant allelic frequency analysis.** ***(a)*** Variant allelic
744 frequency of *bona fide* mutations in MEF clones for each irradiation condition. ***(b)*** Variant allelic
745 frequency of *bona fide* mutations in HFF clones for each irradiation condition.
746
747 **Supplementary Figure 7. Mutation analysis of UV-treated MEF and HFF clones and**
748 **PCAWG samples.** ***(a)*** Mutational signature mSBS_N3 identified *in vivo* in mouse models. ***(b)***
749 COSMIC signatures assigned to MEF clones per condition (control, acute and chronic). **(*c*)**
750 Mutational signatures reconstruction of MEF mutational patterns. Accuracy is measured in cosine
751 similarity between the original pattern of a sample and the pattern of a sample reconstructed using
752 the assigned mutational signatures. **(*d*)** COSMIC signatures assigned to HFF clones per condition
753 (control, acute and chronic). **(*e*)** Mutational signatures reconstruction of HFF mutational patterns.
754 **(*f*)** COSMIC signatures assigned to UV-irradiated HEKa cells and control, grouped by SBS18/36
755 and other signatures. Numbers reflect the number of somatic mutations assigned to the signatures
756 (upper track). Percentages reflect the number of somatic mutations assigned to the signatures
757 divided by the total number of mutations (lower track). **(*g*)** Mutational signatures reconstruction
758 of HEKa mutational patterns. **(*h*)** Correlation analysis of C>A and C>T mutations using PCAWG
759 (whole-genome) and TCGA (whole-exome) data of skin cancer samples. **(*i*)** Percentage
760 contribution of the C>A mutations to SBS18/36 in PCAWG and TCGA skin cancer samples.
761
762 **Supplementary Figure 8. Toxicity and characteristics of the UV-nail polish dryer machine.**
763 ***(a)*** Intensity of UV radiation (mW/cm^2) at different position points (vertical and horizontal) in the
764 employed UV nail polish dryer. ***(b)*** Stability assessment of the UV intensity emitted from the UV-
765 nail polish dryer over time.
766

767 **ACKNOWLEDGEMENTS**

768 The authors would like to thank Dr. John Murray (Indiana University Bloomington) for
769 providing human foreskin fibroblasts. This work was supported by Alfred P. Sloan Research
770 Fellowship. LBA is also an Abeloff V scholar and he is personally supported by a Packard
771 Fellowship for Science and Engineering. This work was also supported by the US National
772 Institute of Health grants R01ES030993-01A1, R01ES032547-01, and R01CA269919-01 to
773 LBA as well as R35ES031638-03 to BVH. The funders had no roles in study design, data
774 collection and analysis, decision to publish, or preparation of the manuscript.

775

776 **AUTHOR CONTRIBUTIONS**

777 LBA and MZ designed all experiments with help from BVH. MZ performed all experiments
778 with assistance from AH, NV and YY. MZ performed all data analysis with help from CY, JD,
779 and YH. BVH assisted in the writing of the manuscript and helped interpreting the experimental
780 results. The manuscript was written by LBA and MZ with input from all other authors. LBA
781 supervised the overall project and writing of the manuscript. All authors read and approved the
782 final manuscript.

783

784 **COMPETING INTERESTS**

785 LBA is a compensated consultant and has equity interest in io9, LLC. His spouse is an employee
786 of Biotheranostics, Inc. LBA is also an inventor of a US Patent 10,776,718 for source identification
787 by non-negative matrix factorization. LBA declares provisional patent applications for "Clustered
788 mutations for the treatment of cancer" (U.S. provisional application serial number 63/289,601),
789 "Artificial intelligence architecture for predicting cancer biomarker" (serial number 63/269,033),

790 “Methods and systems for detecting homologous recombination deficiency in cancer therapies”
791 (serial number 63/366,392), and “Drugs for treating head and neck cancers with chromosome 9p
792 loss” (serial number 63/367,846). All other authors declare no competing interests.
793

794 **DATA AVAILABILITY**

795 All whole-genome and duplex sequencing data have been deposited to Sequence Read Archive
796 (SRA) and can be downloaded using accession number: PRJNA667106.
797

REFERENCES

1 Khan, A. Q., Travers, J. B. & Kemp, M. G. Roles of UVA radiation and DNA damage responses in melanoma pathogenesis. *Environ Mol Mutagen* **59**, 438-460, doi:10.1002/em.22176 (2018).

2 Pfeifer, G. P. Mechanisms of UV-induced mutations and skin cancer. *Genome Instab Dis* **1**, 99-113, doi:10.1007/s42764-020-00009-8 (2020).

3 You, Y. H., Szabó, P. E. & Pfeifer, G. P. Cyclobutane pyrimidine dimers form preferentially at the major p53 mutational hotspot in UVB-induced mouse skin tumors. *Carcinogenesis* **21**, 2113-2117, doi:10.1093/carcin/21.11.2113 (2000).

4 Pfeifer, G. P. Formation and processing of UV photoproducts: effects of DNA sequence and chromatin environment. *Photochem Photobiol* **65**, 270-283, doi:10.1111/j.1751-1097.1997.tb08560.x (1997).

5 Cadet, J. *et al.* Effects of UV and visible radiation on DNA-final base damage. *Biol Chem* **378**, 1275-1286 (1997).

6 Cadet, J., Douki, T. & Ravanat, J. L. Oxidatively generated damage to cellular DNA by UVB and UVA radiation. *Photochem Photobiol* **91**, 140-155, doi:10.1111/php.12368 (2015).

7 Zhang, X. *et al.* Induction of 8-oxo-7,8-dihydro-2'-deoxyguanosine by ultraviolet radiation in calf thymus DNA and HeLa cells. *Photochem Photobiol* **65**, 119-124, doi:10.1111/j.1751-1097.1997.tb01886.x (1997).

8 Besaratinia, A. *et al.* DNA lesions induced by UV A1 and B radiation in human cells: comparative analyses in the overall genome and in the p53 tumor suppressor gene. *Proc Natl Acad Sci U S A* **102**, 10058-10063, doi:10.1073/pnas.0502311102 (2005).

9 Schuch, A. P., Moreno, N. C., Schuch, N. J., Menck, C. F. M. & Garcia, C. C. M. Sunlight damage to cellular DNA: Focus on oxidatively generated lesions. *Free Radic Biol Med* **107**, 110-124, doi:10.1016/j.freeradbiomed.2017.01.029 (2017).

10 Brem, R., Li, F. & Karran, P. Reactive oxygen species generated by thiopurine/UVA cause irreparable transcription-blocking DNA lesions. *Nucleic Acids Res* **37**, 1951-1961, doi:10.1093/nar/gkp070 (2009).

11 Douki, T. & Sage, E. Dewar valence isomers, the third type of environmentally relevant DNA photoproducts induced by solar radiation. *Photochem Photobiol Sci* **15**, 24-30, doi:10.1039/c5pp00382b (2016).

12 Rochette, P. J. *et al.* UVA-induced cyclobutane pyrimidine dimers form predominantly at thymine-thymine dipyrimidines and correlate with the mutation spectrum in rodent cells. *Nucleic Acids Res* **31**, 2786-2794, doi:10.1093/nar/gkg402 (2003).

13 El Ghissassi, F. *et al.* A review of human carcinogens--part D: radiation. *Lancet Oncol* **10**, 751-752, doi:10.1016/s1470-2045(09)70213-x (2009).

14 Sample, A. & He, Y. Y. Mechanisms and prevention of UV-induced melanoma. *Photodermatol Photoimmunol Photomed* **34**, 13-24, doi:10.1111/phpp.12329 (2018).

15 cancer, I. A. f. R. o. C. W. G. o. a. u. U. l. a. s. The association of use of sunbeds with cutaneous malignant melanoma and other skin cancers: A systematic review. *Int J Cancer* **120**, 1116-1122, doi:10.1002/ijc.22453 (2007).

16 van Weelden, H., de Gruijl, F. R., van der Putte, S. C., Toonstra, J. & van der Leun, J. C. The carcinogenic risks of modern tanning equipment: is UV-A safer than UV-B? *Arch Dermatol Res* **280**, 300-307, doi:10.1007/bf00440604 (1988).

843 17 van Weelden, H., van der Putte, S. C., Toonstra, J. & van der Leun, J. C. UVA-induced
844 tumours in pigmented hairless mice and the carcinogenic risks of tanning with UVA. *Arch*
845 *Dermatol Res* **282**, 289-294, doi:10.1007/bf00375721 (1990).
846 18 Sterenborg, H. J. & van der Leun, J. C. Tumorigenesis by a long wavelength UV-A source.
847 *Photochem Photobiol* **51**, 325-330, doi:10.1111/j.1751-1097.1990.tb01718.x (1990).
848 19 Kelfkens, G., de Gruijl, F. R. & van der Leun, J. C. Tumorigenesis by short-wave
849 ultraviolet A: papillomas versus squamous cell carcinomas. *Carcinogenesis* **12**, 1377-
850 1382, doi:10.1093/carcin/12.8.1377 (1991).
851 20 Greinert, R. *et al.* UVA-induced DNA double-strand breaks result from the repair of
852 clustered oxidative DNA damages. *Nucleic Acids Res* **40**, 10263-10273,
853 doi:10.1093/nar/gks824 (2012).
854 21 Didier, C., Emonet-Piccardi, N., Béani, J. C., Cadet, J. & Richard, M. J. L-arginine
855 increases UVA cytotoxicity in irradiated human keratinocyte cell line: potential role of
856 nitric oxide. *FASEB J* **13**, 1817-1824, doi:10.1096/fasebj.13.13.1817 (1999).
857 22 Francis, A. J. & Giannelli, F. Cooperation between human cells sensitive to UVA
858 radiations: a clue to the mechanism of cellular hypersensitivity associated with different
859 clinical conditions. *Exp Cell Res* **195**, 47-52, doi:10.1016/0014-4827(91)90498-j (1991).
860 23 Eisenstark, A. Mutagenic and lethal effects of near-ultraviolet radiation (290-400 nm) on
861 bacteria and phage. *Environ Mol Mutagen* **10**, 317-337, doi:10.1002/em.2850100311
862 (1987).
863 24 Ridley, A. J., Whiteside, J. R., McMillan, T. J. & Allinson, S. L. Cellular and sub-cellular
864 responses to UVA in relation to carcinogenesis. *Int J Radiat Biol* **85**, 177-195,
865 doi:10.1080/09553000902740150 (2009).
866 25 Besaratinia, A., Bates, S. E., Synold, T. W. & Pfeifer, G. P. Similar mutagenicity of
867 photoactivated porphyrins and ultraviolet A radiation in mouse embryonic fibroblasts:
868 involvement of oxidative DNA lesions in mutagenesis. *Biochemistry* **43**, 15557-15566,
869 doi:10.1021/bi048717c (2004).
870 26 Besaratinia, A., Kim, S. I., Bates, S. E. & Pfeifer, G. P. Riboflavin activated by ultraviolet
871 A1 irradiation induces oxidative DNA damage-mediated mutations inhibited by vitamin C.
872 *Proc Natl Acad Sci U S A* **104**, 5953-5958, doi:10.1073/pnas.0610534104 (2007).
873 27 Kim, S. I., Pfeifer, G. P. & Besaratinia, A. Mutagenicity of ultraviolet A radiation in the
874 lacI transgene in Big Blue mouse embryonic fibroblasts. *Mutat Res* **617**, 71-78,
875 doi:10.1016/j.mrfmmm.2006.12.003 (2007).
876 28 Pfeifer, G. P., You, Y. H. & Besaratinia, A. Mutations induced by ultraviolet light. *Mutat*
877 *Res* **571**, 19-31, doi:10.1016/j.mrfmmm.2004.06.057 (2005).
878 29 Rieder, E. A. & Tosti, A. Cosmetically Induced Disorders of the Nail with Update on
879 Contemporary Nail Manicures. *J Clin Aesthet Dermatol* **9**, 39-44 (2016).
880 30 Bollard, S. M. *et al.* Skin cancer risk and the use of UV nail lamps. *Australas J Dermatol*
881 **59**, 348-349, doi:10.1111/ajd.12806 (2018).
882 31 Shipp, L. R., Warner, C. A., Rueggeberg, F. A. & Davis, L. S. Further investigation into
883 the risk of skin cancer associated with the use of UV nail lamps. *JAMA Dermatol* **150**, 775-
884 776, doi:10.1001/jamadermatol.2013.8740 (2014).
885 32 Ratycz, M. C., Lender, J. A. & Gottwald, L. D. Multiple Dorsal Hand Actinic Keratoses
886 and Squamous Cell Carcinomas: A Unique Presentation following Extensive UV Nail
887 Lamp Use. *Case Rep Dermatol* **11**, 286-291, doi:10.1159/000503273 (2019).

33 Ceballos, D. M. *et al.* Biological and environmental exposure monitoring of volatile organic compounds among nail technicians in the Greater Boston area. *Indoor Air* **29**, 539-550, doi:10.1111/ina.12564 (2019).

34 MacFarlane, D. F. & Alonso, C. A. Occurrence of nonmelanoma skin cancers on the hands after UV nail light exposure. *Arch Dermatol* **145**, 447-449, doi:10.1001/archdermatol.2008.622 (2009).

35 Zhivagui, M., Korenjak, M. & Zavadil, J. Modelling Mutation Spectra of Human Carcinogens Using Experimental Systems. *Basic Clin Pharmacol Toxicol* **121 Suppl 3**, 16-22, doi:10.1111/bcpt.12690 (2017).

36 Schmitt, M. W. *et al.* Detection of ultra-rare mutations by next-generation sequencing. *Proc Natl Acad Sci U S A* **109**, 14508-14513, doi:10.1073/pnas.1208715109 (2012).

37 Sharma, A., Singh, K. & Almasan, A. Histone H2AX phosphorylation: a marker for DNA damage. *Methods Mol Biol* **920**, 613-626, doi:10.1007/978-1-61779-998-3_40 (2012).

38 Budden, T. & Bowden, N. A. The role of altered nucleotide excision repair and UVB-induced DNA damage in melanomagenesis. *Int J Mol Sci* **14**, 1132-1151, doi:10.3390/ijms14011132 (2013).

39 Yang, Z. & Choi, H. Single-Cell, Time-Lapse Reactive Oxygen Species Detection in E. coli. *Curr Protoc Cell Biol* **80**, e60, doi:10.1002/cpcb.60 (2018).

40 Suzuki, T. & Kamiya, H. Mutations induced by 8-hydroxyguanine (8-oxo-7,8-dihydroguanine), a representative oxidized base, in mammalian cells. *Genes Environ* **39**, 2, doi:10.1186/s41021-016-0051-y (2017).

41 Douki, T. *et al.* Oxidation of guanine in cellular DNA by solar UV radiation: biological role. *Photochem Photobiol* **70**, 184-190 (1999).

42 KESTON, A. S. & BRANDT, R. THE FLUOROMETRIC ANALYSIS OF ULTRAMICRO QUANTITIES OF HYDROGEN PEROXIDE. *Anal Biochem* **11**, 1-5, doi:10.1016/0003-2697(65)90034-5 (1965).

43 Ezeriņa, D., Takano, Y., Hanaoka, K., Urano, Y. & Dick, T. P. N-Acetyl Cysteine Functions as a Fast-Acting Antioxidant by Triggering Intracellular H. *Cell Chem Biol* **25**, 447-459.e444, doi:10.1016/j.chembiol.2018.01.011 (2018).

44 BRANDT, R. & KESTON, A. S. SYNTHESIS OF DIACETYLDICHLOROFLUORESCIN: A STABLE REAGENT FOR FLUOROMETRIC ANALYSIS. *Anal Biochem* **11**, 6-9, doi:10.1016/0003-2697(65)90035-7 (1965).

45 Bass, D. A. *et al.* Flow cytometric studies of oxidative product formation by neutrophils: a graded response to membrane stimulation. *J Immunol* **130**, 1910-1917 (1983).

46 Murphy, M. P. How mitochondria produce reactive oxygen species. *Biochem J* **417**, 1-13, doi:10.1042/BJ20081386 (2009).

47 Brand, R. M. *et al.* Targeting Mitochondrial Oxidative Stress to Mitigate UV-Induced Skin Damage. *Front Pharmacol* **9**, 920, doi:10.3389/fphar.2018.00920 (2018).

48 Zhivagui, M. *et al.* Experimental and pan-cancer genome analyses reveal widespread contribution of acrylamide exposure to carcinogenesis in humans. *Genome Res* **29**, 521-531, doi:10.1101/gr.242453.118 (2019).

49 Salk, J. J., Schmitt, M. W. & Loeb, L. A. Enhancing the accuracy of next-generation sequencing for detecting rare and subclonal mutations. *Nat Rev Genet* **19**, 269-285, doi:10.1038/nrg.2017.117 (2018).

50 Salk, J. J. & Kennedy, S. R. Next-Generation Genotoxicology: Using Modern Sequencing Technologies to Assess Somatic Mutagenesis and Cancer Risk. *Environ Mol Mutagen* **61**, 135-151, doi:10.1002/em.22342 (2020).
51 Abbasi, A. & Alexandrov, L. B. Significance and limitations of the use of next-generation sequencing technologies for detecting mutational signatures. *DNA Repair (Amst)* **107**, 103200, doi:10.1016/j.dnarep.2021.103200 (2021).
52 Alexandrov, L. B. *et al.* Signatures of mutational processes in human cancer. *Nature* **500**, 415-421, doi:10.1038/nature12477 (2013).
53 Alexandrov, L. B. & Stratton, M. R. Mutational signatures: the patterns of somatic mutations hidden in cancer genomes. *Curr Opin Genet Dev* **24**, 52-60, doi:10.1016/j.gde.2013.11.014 (2014).
54 Alexandrov, L. B. & Zhivagui, M. in *Encyclopedia of Cancer (Third Edition)* 499-510 (2019).
55 Alexandrov, L. B., Nik-Zainal, S., Wedge, D. C., Campbell, P. J. & Stratton, M. R. Deciphering signatures of mutational processes operative in human cancer. *Cell Rep* **3**, 246-259, doi:10.1016/j.celrep.2012.12.008 (2013).
56 Riva, L. *et al.* The mutational signature profile of known and suspected human carcinogens in mice. *Nat Genet* **52**, 1189-1197, doi:10.1038/s41588-020-0692-4 (2020).
57 Pilati, C. *et al.* Mutational signature analysis identifies MUTYH deficiency in colorectal cancers and adrenocortical carcinomas. *J Pathol* **242**, 10-15, doi:10.1002/path.4880 (2017).
58 Viel, A. *et al.* A Specific Mutational Signature Associated with DNA 8-Oxoguanine Persistence in MUTYH-defective Colorectal Cancer. *EBioMedicine* **20**, 39-49, doi:10.1016/j.ebiom.2017.04.022 (2017).
59 Georgeson, P. *et al.* Identifying colorectal cancer caused by biallelic MUTYH pathogenic variants using tumor mutational signatures. *Nat Commun* **13**, 3254, doi:10.1038/s41467-022-30916-1 (2022).
60 Levatić, J., Salvadores, M., Fuster-Tormo, F. & Supek, F. Mutational signatures are markers of drug sensitivity of cancer cells. *Nat Commun* **13**, 2926, doi:10.1038/s41467-022-30582-3 (2022).
61 Georgeson, P. *et al.* Evaluating the utility of tumour mutational signatures for identifying hereditary colorectal cancer and polyposis syndrome carriers. *Gut* **70**, 2138-2149, doi:10.1136/gutjnl-2019-320462 (2021).
62 Alexandrov, L. B. *et al.* The repertoire of mutational signatures in human cancer. *Nature* **578**, 94-101, doi:10.1038/s41586-020-1943-3 (2020).
63 Trucco, L. D. *et al.* Ultraviolet radiation-induced DNA damage is prognostic for outcome in melanoma. *Nat Med* **25**, 221-224, doi:10.1038/s41591-018-0265-6 (2019).
64 Moreno, N. C. *et al.* Whole-exome sequencing reveals the impact of UVA light mutagenesis in xeroderma pigmentosum variant human cells. *Nucleic Acids Res* **48**, 1941-1953, doi:10.1093/nar/gkz1182 (2020).
65 Feigelson, H. S. *et al.* Melanoma incidence, recurrence, and mortality in an integrated healthcare system: A retrospective cohort study. *Cancer Med* **8**, 4508-4516, doi:10.1002/cam4.2252 (2019).
66 Ferlay, J. *et al.* Estimating the global cancer incidence and mortality in 2018: GLOBOCAN sources and methods. *Int J Cancer* **144**, 1941-1953, doi:10.1002/ijc.31937 (2019).

67 Weir, H. K. *et al.* Melanoma in adolescents and young adults (ages 15-39 years): United States, 1999-2006. *J Am Acad Dermatol* **65**, S38-49, doi:10.1016/j.jaad.2011.04.038 (2011).
68 Tomasetti, C., Marchionni, L., Nowak, M. A., Parmigiani, G. & Vogelstein, B. Only three driver gene mutations are required for the development of lung and colorectal cancers. *Proc Natl Acad Sci U S A* **112**, 118-123, doi:10.1073/pnas.1421839112 (2015).
69 Tomasetti, C., Li, L. & Vogelstein, B. Stem cell divisions, somatic mutations, cancer etiology, and cancer prevention. *Science* **355**, 1330-1334, doi:10.1126/science.aaf9011 (2017).
70 Balmain, A. The critical roles of somatic mutations and environmental tumor-promoting agents in cancer risk. *Nat Genet* **52**, 1139-1143, doi:10.1038/s41588-020-00727-5 (2020).
71 Zhang, M. *et al.* Use of tanning beds and incidence of skin cancer. *J Clin Oncol* **30**, 1588-1593, doi:10.1200/JCO.2011.39.3652 (2012).
72 O'Sullivan, N. A. & Tait, C. P. Tanning bed and nail lamp use and the risk of cutaneous malignancy: a review of the literature. *Australas J Dermatol* **55**, 99-106, doi:10.1111/ajd.12145 (2014).
73 Consortium, I. T. P.-C. A. o. W. G. Pan-cancer analysis of whole genomes. *Nature* **578**, 82-93, doi:10.1038/s41586-020-1969-6 (2020).
74 Ellrott, K. *et al.* Scalable Open Science Approach for Mutation Calling of Tumor Exomes Using Multiple Genomic Pipelines. *Cell Syst* **6**, 271-281.e277, doi:10.1016/j.cels.2018.03.002 (2018).
75 David Benjamin *et al.* (bioRxiv 2019).
76 Koboldt, D. C., Larson, D. E. & Wilson, R. K. Using VarScan 2 for Germline Variant Calling and Somatic Mutation Detection. *Curr Protoc Bioinformatics* **44**, 15.14.11-17, doi:10.1002/0471250953.bi1504s44 (2013).
77 Kim, S. *et al.* Strelka2: fast and accurate calling of germline and somatic variants. *Nat Methods* **15**, 591-594, doi:10.1038/s41592-018-0051-x (2018).
78 Fan, Y. *et al.* MuSE: accounting for tumor heterogeneity using a sample-specific error model improves sensitivity and specificity in mutation calling from sequencing data. *Genome Biol* **17**, 178, doi:10.1186/s13059-016-1029-6 (2016).
79 McLaren, W. *et al.* The Ensembl Variant Effect Predictor. *Genome Biol* **17**, 122, doi:10.1186/s13059-016-0974-4 (2016).
80 Bergstrom, E. N. *et al.* SigProfilerMatrixGenerator: a tool for visualizing and exploring patterns of small mutational events. *BMC Genomics* **20**, 685, doi:10.1186/s12864-019-6041-2 (2019).
81 Bergstrom, E. N., Barnes, M., Martincorena, I. & Alexandrov, L. B. Generating realistic null hypothesis of cancer mutational landscapes using SigProfilerSimulator. *BMC Bioinformatics* **21**, 438, doi:10.1186/s12859-020-03772-3 (2020).
82 Thorvaldsdóttir, H., Robinson, J. T. & Mesirov, J. P. Integrative Genomics Viewer (IGV): high-performance genomics data visualization and exploration. *Brief Bioinform* **14**, 178-192, doi:10.1093/bib/bbs017 (2013).
83 Gu, Z., Eils, R. & Schlesner, M. Complex heatmaps reveal patterns and correlations in multidimensional genomic data. *Bioinformatics* **32**, 2847-2849, doi:10.1093/bioinformatics/btw313 (2016).

84 Gu, Z., Gu, L., Eils, R., Schlesner, M. & Brors, B. circlize Implements and enhances circular visualization in R. *Bioinformatics* **30**, 2811-2812, doi:10.1093/bioinformatics/btu393 (2014).

85 Günther, F., Dudschig, C. & Kaup, B. LSAfun--An R package for computations based on Latent Semantic Analysis. *Behav Res Methods* **47**, 930-944, doi:10.3758/s13428-014-0529-0 (2015).

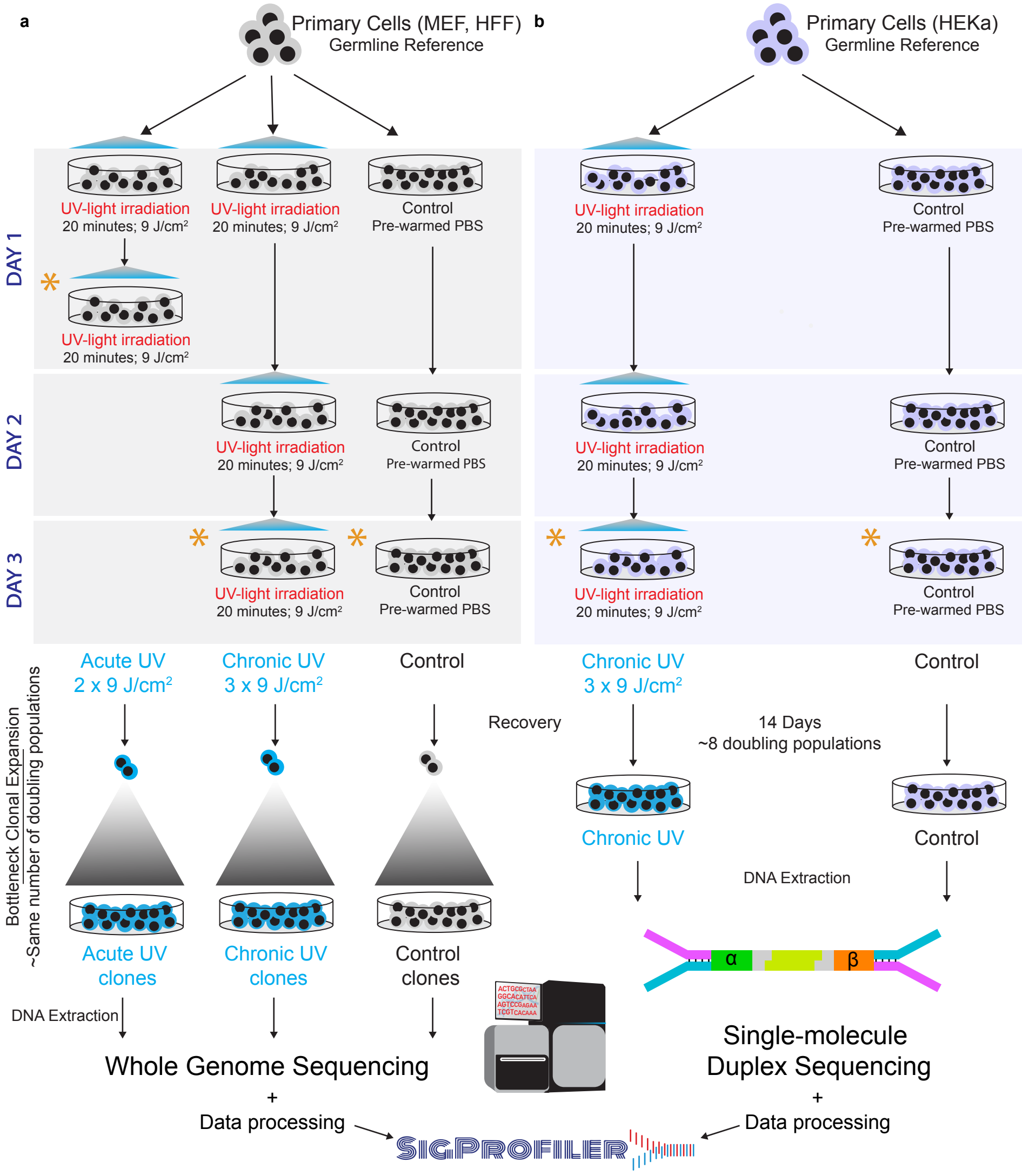

c

UV-light irradiation using a UV-nail polish dryer

Barrier bypass-clonal expansion

✳ Experimental assays

Assessment	Assays	Timepoint
Cytotoxicity	Cell Counting kit (CCK-8)	48h
	Trypan Blue	
Genotoxicity	γH2Ax immunofluorescence	4h
	CPD/6-4PP immunofluorescence	Immediately
Oxidative damage	CellROX green reagent	Immediately
	OxiSelect In vitro ROS/RNS assay kit	Immediately
		20min
		24h
	EpiQuik 8-OHdG DNA damage quantification kit	Immediately
		4h
		24h
Mitochondrial damage	MitoSOX mitochondrial superoxide indicator	24h
	TMRM mitochondrial membrane potential indicator	

Figure 1

Figure 2

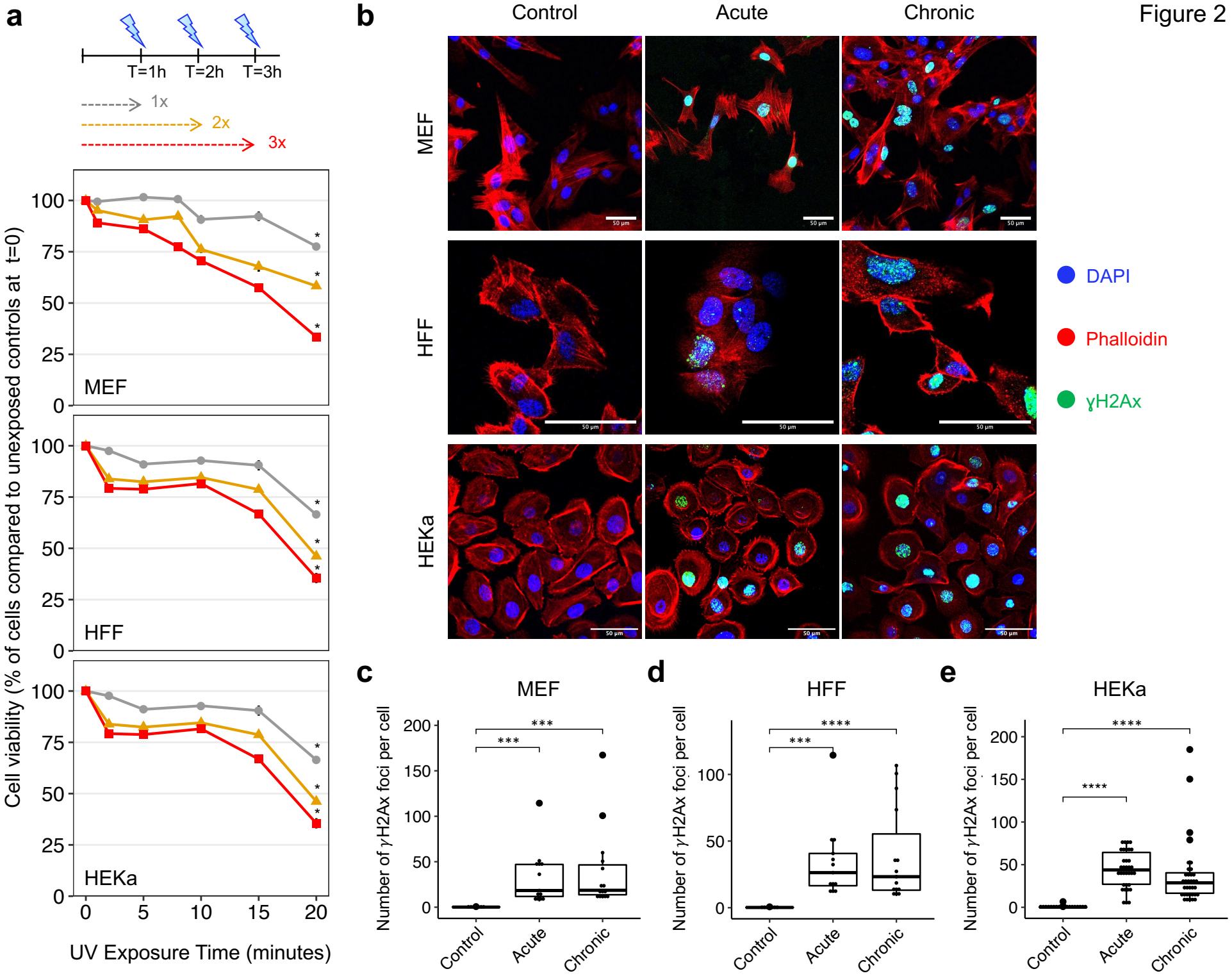
a
T=1h
T=2h
T=3h
1x
2x
3x
Cell viability (% of cells compared to unexposed controls at t=0)
MEF
HFF
HEKa
UV Exposure Time (minutes)
b
Control
Acute
Chronic
MEF
HFF
HEKa
DAPI
Phalloidin
γH2Ax
c
MEF
d
HFF
e
HEKa
Number of γH2Ax foci per cell
Control
Acute
Chronic

Figure 3

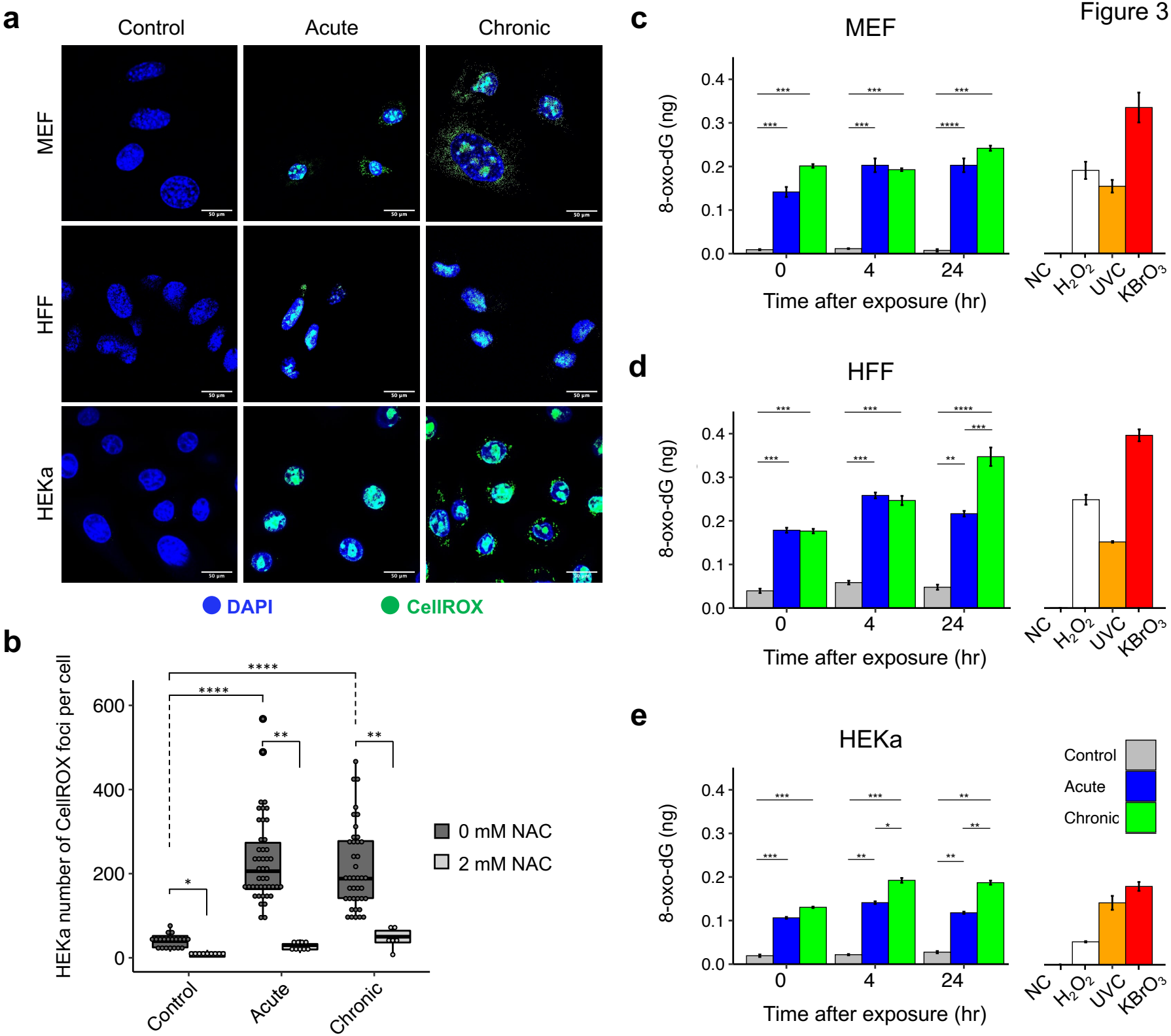
a
Control
Acute
Chronic
MEF
HFF
HEKa
DAPI
CellROX
b
HEKa number of CellROX foci per cell
0 mM NAC
2 mM NAC
Control
Acute
Chronic
c
MEF
8-oxo-dG (ng)
Time after exposure (hr)
NC
H2O2
UVC
KBrO3
d
HFF
e
HEKa
Control
Acute
Chronic

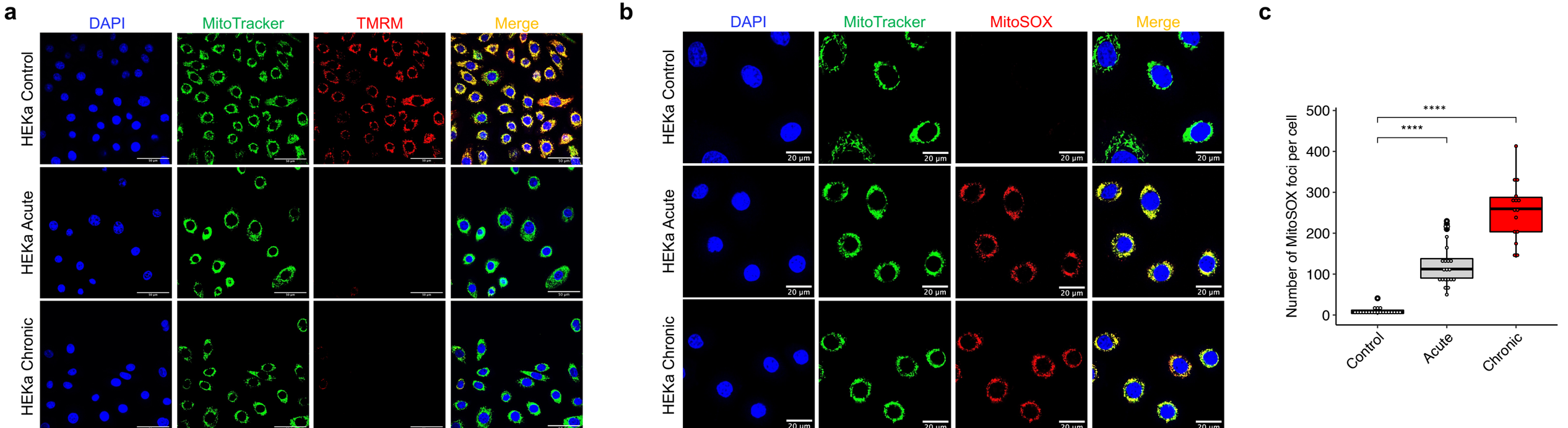
a
DAPI
MitoTracker
TMRM
Merge
HEKa Control
HEKa Acute
HEKa Chronic
b
DAPI
MitoTracker
MitoSOX
Merge
HEKa Control
HEKa Acute
HEKa Chronic
20 µm
c
Number of MitoSOX foci per cell
500
400
300
200
100
0
****
****
Control
Acute
Chronic

Figure 4

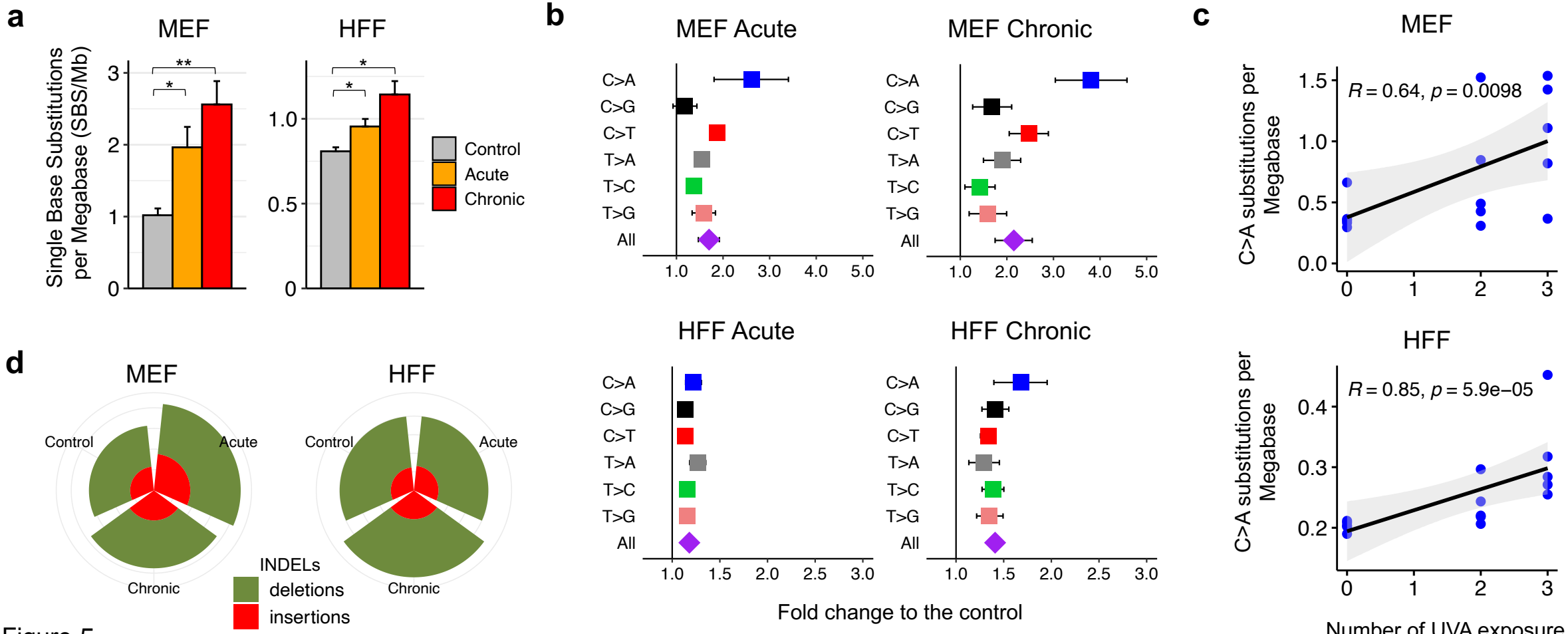
a
MEF
HFF
Single Base Substitutions per Megabase (SBS/Mb)
Control
Acute
Chronic
b
MEF Acute
MEF Chronic
HFF Acute
HFF Chronic
C>A
C>G
C>T
T>A
T>C
T>G
All
Fold change to the control
c
MEF
HFF
C>A substitutions per Megabase
R = 0.64, p = 0.0098
R = 0.85, p = 5.9e−05
Number of UVA exposure
d
MEF
HFF
Control
Acute
Chronic
INDELs
deletions
insertions

Figure 5

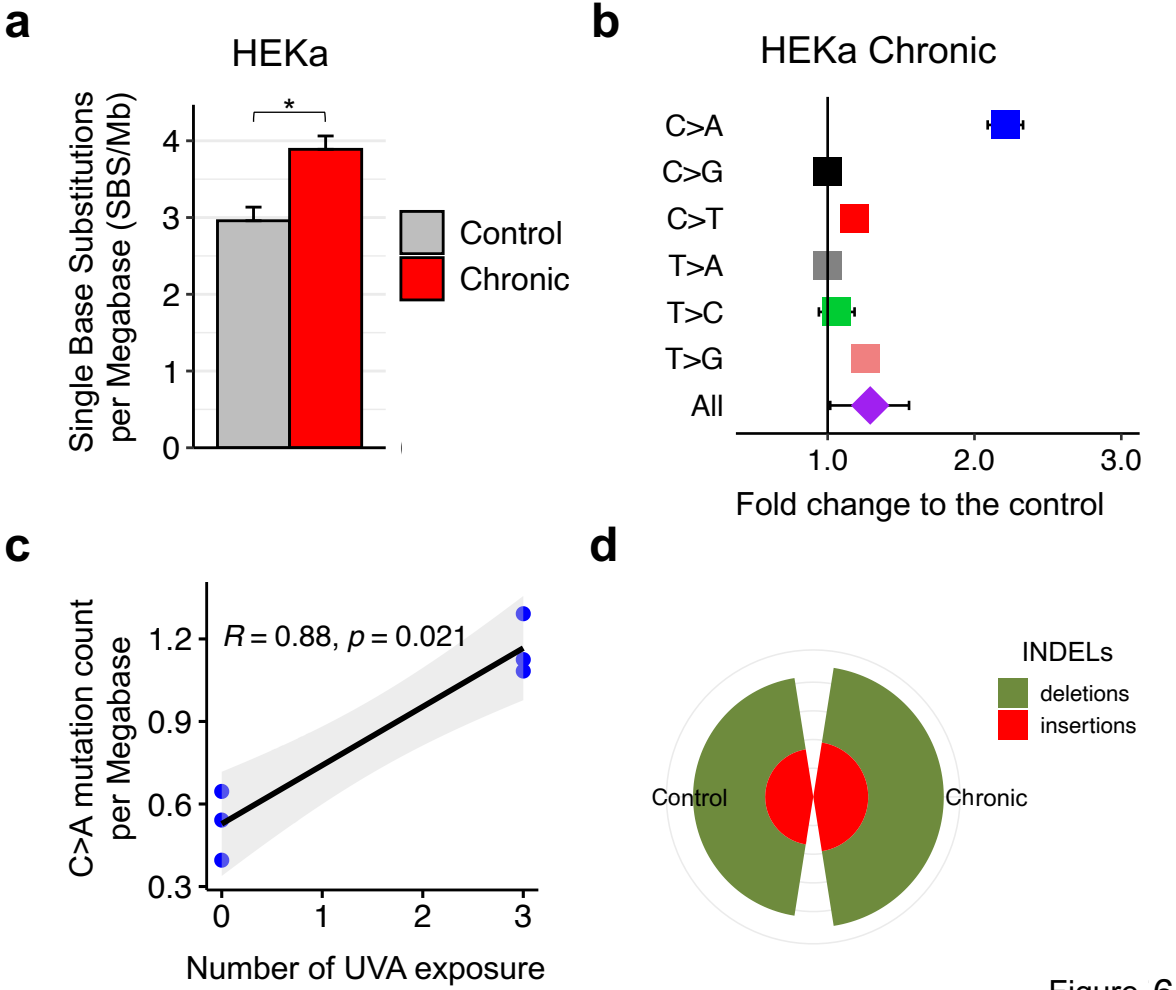
a
HEKa
Single Base Substitutions per Megabase (SBS/Mb)
*
0
1
2
3
4
Control
Chronic
b
HEKa Chronic
C>A
C>G
C>T
T>A
T>C
T>G
All
1.0
2.0
3.0
Fold change to the control
c
C>A mutation count per Megabase
R = 0.88, p = 0.021
0.3
0.6
0.9
1.2
0
1
2
3
Number of UVA exposure
d
INDELs
deletions
insertions
Control
Chronic

Figure 6

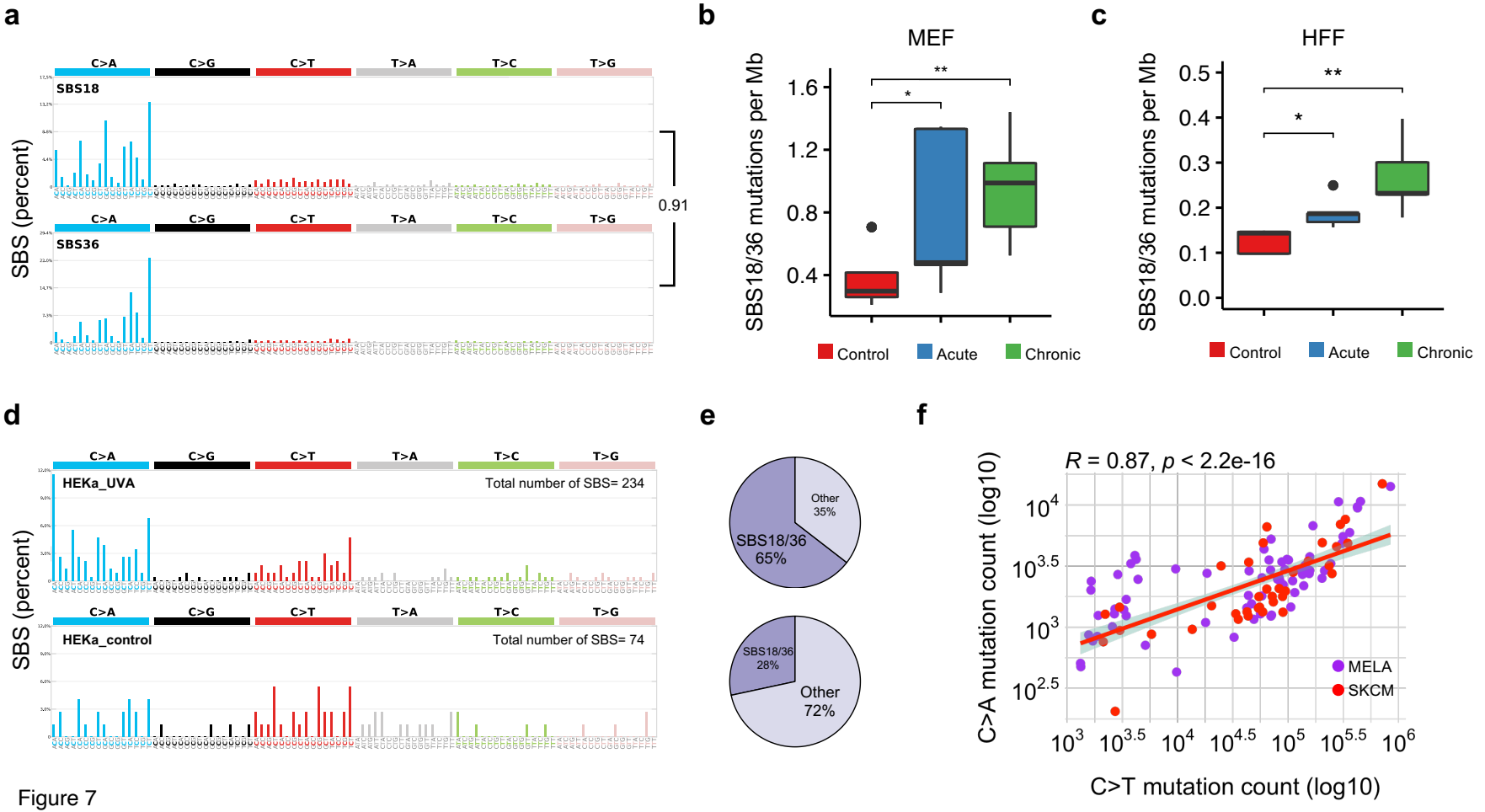
a
C>A
C>G
C>T
T>A
T>C
T>G
SBS18
SBS36
SBS (percent)
0.91
b
MEF
SBS18/36 mutations per Mb
1.6
1.2
0.8
0.4
**
*
Control
Acute
Chronic
c
HFF
SBS18/36 mutations per Mb
0.5
0.4
0.3
0.2
0.1
0.0
**
*
Control
Acute
Chronic
d
HEKa_UVA
Total number of SBS= 234
HEKa_control
Total number of SBS= 74
SBS (percent)
e
SBS18/36
65%
Other
35%
SBS18/36
28%
Other
72%
f
R = 0.87, p < 2.2e-16
C>A mutation count (log10)
C>T mutation count (log10)
MELA
SKCM

Figure 7